Investigation Into the Use of Single Inductor for Driving Multiple Series-Connected LED Channels

Xiaoqing Zhan, *Student Member, IEEE*, Henry Chung, *Fellow, IEEE*, and Ruihong Zhang, *Member, IEEE*

***Abstract*—An investigation into the use of single inductor for driving *N* series-connected LED channels is presented. Each channel has a parallel-connected switch for controlling the LED channel current, as well as charging the inductor. Compared with the conventional structure having all LED channels connected in parallel and $(N+1)$ switches, the proposed structure has the merits of 1) requiring *N* switches, 2) allowing all channels to be driven concurrently in every switching cycle, and 3) being insensitive to the duration of the transition switching from one channel to another. Detailed mathematical analysis on the topological operations will be discussed. The proposed concept will be demonstrated on a two-channel structure. A prototype with two 7 W LED modules has been built and evaluated. A control mechanism that can regulate the output luminous flux and correlated color temperature without sensing the inductor current and channel currents will be discussed. Experimental results are favorably compared with theoretical predictions.**

***Index Terms*—DC–DC power conversion, lighting, lighting control, single-inductor-multiple-output (SIMO) power conversion.**

NOMENCLATURE

α	Transformation variable from the electrical analysis to optical analysis.
η_i	Luminous efficacy of the LED Channel *i*.
$\phi_{s,i}$	Luminous flux emitted by the LED Channel *i*.
Φ_o	Output luminous flux of the LED lamp.
$\Phi_{\rm ref}$	Luminous flux reference.
CCT	Correlated color temperature.
$\rm CCT_o$	CCT of the output of the LED lamp.
$\rm CCT_{ref}$:	CCT reference.
ε_1	Error between $\Phi_{\rm ref}$ and Φ_o.
ε_2	Error between $\rm CCT_{ref}$ and $\rm CCT_o$.
$D_{\rm warm}$	Diode in series with the warm LED channel.
$D_{\rm cool}$	Diode in series with the cool LED channel.
d_k	Duty cycle of mode *k*.
$D_{s,i}$	Diode in series with LED channel *i*.
E	Total energy consumed by all LED channels during one switching cycle.
$E_{\rm warm}$	Energy consumed by the warm LED channel during one switching cycle.
$E_{\rm cool}$	Energy consumed by the cool LED channel during one switching cycle.
$E_{s,i}$	Energy consumed by LED channel *i* during one switching cycle.
$I_{\rm dc}$	Average input current.
$i_{\rm cool}$	Current of cool LED channel.
i_L	Current of the inductor.
$i_{\rm warm}$	Current of warm LED channel.
$I_{L,k}$	Initial current of the inductor in mode *k*.
$\bar{I}_{L,k}$	Average current of the inductor in mode *k*.
$K_{i,1}$	Integral gain of the flux control loop.
$K_{i,2}$	Integral gain of the CCT control loop.
$K_{p,1}$	Proportional gain of the flux control loop.
$K_{p,2}$	Proportional gain of the CCT control loop.
L	Inductor.
m	Ratio of duty cycle.
m_i	Initial value of *m*.
Q_i	MOSFET paralleled with LED channel *i*.
$Q_{\rm cool}$	MOSFET paralleled with the cool LED channel.
$Q_{\rm warm}$	MOSFET paralleled with the warm LED channel.
t_k	Start time of mode *k*.
t_{k+1}	End time of mode *k*.
Δt_k	Duration of mode *k*.
$\Delta t_{k,i}$	Initial estimation of Δt_k in the controller.
f_s	Switching frequency.
T_s	Switching period $(=1/f_s)$.
$T_{\rm sam}$	Sampling period.
$V_{\rm in}$	Input voltage.
$V_{s,i}$	Forward voltage of LED channel *i*.
$V_{\rm warm}$	Forward voltage of the warm LED channel.
$V_{\rm cool}$	Forward voltage of the cool LED channel.
$v_{g,Qc}$	Gate signal for the MOSFET connected in parallel with the cool LED channel.
$v_{g,Qw}$	Gate signal for the MOSFET connected in parallel with the warm LED channel.
v_L	Inductor voltage.
$V_{L,k}$	Voltage of the inductor in mode *k*.
$V_{o,k}$	Output voltage in mode *k*.

Manuscript received January 27, 2016; revised April 18, 2016; accepted May 20, 2016. Date of publication June 2, 2016; date of current version January 20, 2017. This work was supported by a grant from the Research Grants Council of the Hong Kong Special Administrative Region, China, under Project CityU 11205115. Part of the results has been submitted for presentation at the *IEEE Energy Conversion Congress and Exposition 2016*. Recommended for publication by Associate Editor J. M. Alonso.

X. Zhan and H. S.-H. Chung are with the Centre for Smart Energy Conversion and Utilization Research, City University of Hong Kong, Tat Chee Avenue, Kowloon Tong 999077, Hong Kong (e-mail:) (e-mail: xiaoqzhan2-c@my.cityu.edu.hk; eeshc@um.cityu.edu.hk).

R. Zhang is with the School of Automation, Northwestern Polytechnical University, Xi'an 710029, China (e-mail: eerhzhang@gmail.com).

Color versions of one or more of the figures in this paper are available online at http://ieeexplore.ieee.org.

Digital Object Identifier 10.1109/TPEL.2016.2576279

I. INTRODUCTION

HIGH-POWER LED lamps contain numerous LEDs or LED modules configured in the form of strings. Each string has several series-connected LEDs or LED modules. Each LED channel comprises several strings [1]. The number of strings and values of the string voltage and string current have to match with the output specifications of the LED driver [2].

The string current control network consists of active devices for regulating the string current [3]–[9]. The active device can be operated in linear or switching mode. In linear mode, the active device is connected in series with the string and is operated in the linear region. By controlling the bias condition of the active device, the string current is regulated by using a current mirror or an individual current sensing [3]–[6]. This method is generally called amplitude modulation dimming. In switching mode, the active device is operated as a switch and is connected either in series or in parallel with the string [7]–[9]. The duty time of the string is controlled by a feedback mechanism through sensing the string current and generating appropriate gate signal to the active device. This method is generally called pulse width modulation (PWM) dimming. The two dimming methods each have their own merits and limitations. In terms of color temperature control, PWM dimming has the advantages of reducing the color change associated with the variation in the LED current.

Various techniques utilizing different kinds of sensors, including current sensors [10]–[14], thermal sensors [15]–[16], and optical sensors [17]–[20], have been proposed to regulate the light output. Wang *et al*. [21] uses both thermal and optical sensors. The key challenge of using current and temperature feedback is to deal with the drift of the optical characteristics of the LEDs, including luminous flux and wavelength, with the measured current and temperature. Furthermore, the temperature dependence of the luminous flux and wavelength are sometimes not known *a priori*. Optical feedback, which directly measures and controls the optical parameters of the light, including luminous flux (Φ) and CCT for bicolor lamps, luminous flux and color coordinates for tricolor or tetracolor lamps, can overcome the above-mentioned issues.

To reduce the form factor of the driver, some techniques utilize single inductor to manage currents of *N* parallel-connected LED channels [10]–[14]. They are typically extended from the concept of single-inductor-multiple-output (SIMO) power conversion methods [22]–[25], which are usually used to deliver multiple output voltages. As LEDs are current-driven devices, the SIMO structures are modified to produce regulated currents to the LED channels. The structures typically consist of $(N+1)$ switches with one of them regulating the inductor current and *N* of them for the *N* channels, respectively. The channels are driven by the inductor in two possible time-division multiplexing strategies. The first one has all LED channels activated sequentially in every switching cycle [10]. The second one has only one LED channel activated in each switching cycle [11]–[14]. The channels are activated sequentially over the switching cycles. Since the inductor current cannot be changed instantly and the instantaneous LED current has to be limited to its rated value [26], prior-arts would face the following operational challenges.

1) As the channels are activated in a time-multiplexed manner, the maximum achievable average channel current decreases as the number of channels increases. Thus, utilization of the LED channels is confined.
2) In [10], due to the output capacitor, the output voltage is momentarily constant during the transition switching from one channel to another. As different LEDs have different forward voltages, current spikes through the channels of low forward voltage will occur, giving rise to EMC and reliability concerns.
3) In [11]–[14], the effective operating frequency of each LED channels is reduced.
4) Multiple current sensors [11], [14], one for each LED channel, are required to regulate the average channel current. In [10], [12]–[13], only one sensing resistor is needed. But sophisticated controller for synchronizing the current sensing and regulation is required.

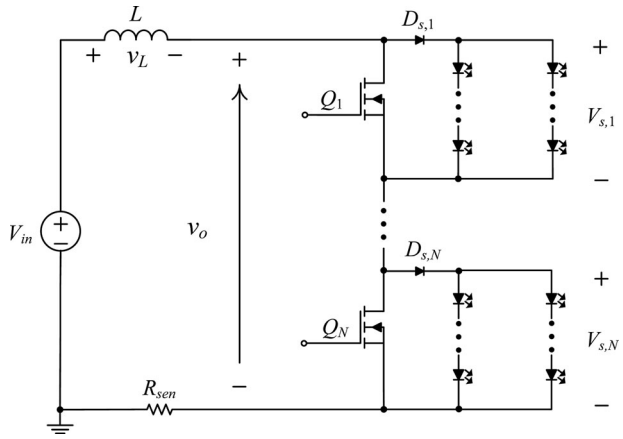

Fig. 1. Single-inductor driver for *N* series-connected LED channels.

Recently, a structure with series-connected LED channels with a front-stage buck converter has been proposed in [27]. However, it requires $(N+2)$ switches, two for regulating the inductor current and *N* for the *N* LED channels. This paper gives another perspective of using single inductor to drive *N* series-connected LED channels. The structure is derived from a boost converter. It has the merits of 1) requiring *N* switches, 2) allowing concurrent driving of all LED channels in every switching cycle, and 3) being insensitive to the transition switching from one channel to another. The concept is demonstrated on a two-channel prototype with optical feedback for regulating luminous flux and CCT. Experimental results are favorably compared with theoretical predictions.

II. Principle of Operations

Fig. 1 shows the generalized structure using single inductor to manage the brightness of *N* LED channels. Each channel consists of multiple parallel-connected LED strings. Each string consists of a series of LEDs. The string currents in each channel are balanced by current balancing techniques [1]. Each channel has a parallel-connected MOSFET. They are $Q_1, \ldots, Q_N$. The series diodes $D_{s,1}, \ldots, D_{s,N}$ are used to limit the channel reverse currents upon turning on the parallel switches. A comparison of the channel currents with and without the series diodes connected will be studied experimentally in Section IV. As the voltage drop of the series diodes is relatively small, as compared to the forward voltage of the LED channels, it is neglected in the following analysis. For the sake of simplicity in the analysis, each LED is assumed to have a constant forward voltage. Let $V_{s,i}$ be the voltage across Channel *i* when the associated MOSFET

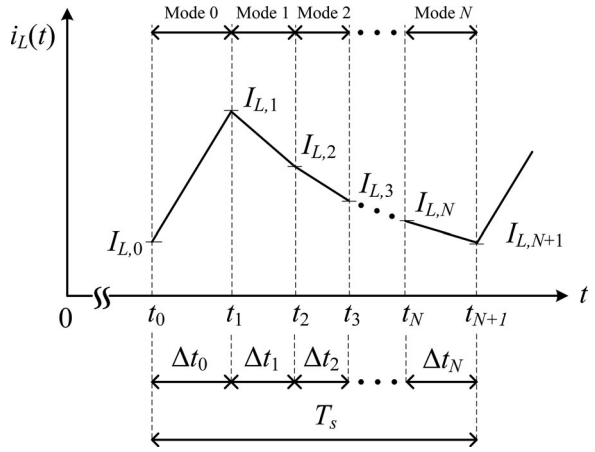

Fig. 2. Waveform of the inductor current in one switching cycle.

is OFF. As shown in Fig. 2, a switching cycle is divided into $N+1$ operating modes. In Mode 0, all MOSFETs are turned ON at t_0 and turned OFF at t_1. Starting from Mode 1, the MOSFETs are switched ON sequentially. All LED channels may have different conduction times. However, considering that the LED channels are connected in series, the channels can be rearranged in the way that Channel 1 has the longest conduction time and Channel *N* has the shortest conduction time. In any case, the LED channel with the longest conduction time in the actual circuit becomes Channel 1 in the analysis. Similarly, the LED channel with the shortest conduction time becomes Channel *N*.

MOSFET Q_N is turned ON at t_2, while MOSFET Q_1 is turned ON at t_{N+1}, end of the switching cycle. Thus, the voltage across the series-connected LED channels in Mode $k, V_{o,k}$, can be expressed as

$$V_{o,k} = \begin{cases} 0, & k = 0 \\ \sum_{i=1}^{N-k+1} V_{s,i}, & k = 1,\ 2, \ldots, N \end{cases}. \tag{1}$$

The operations of the circuit are described as follows.

Mode 0, $t \in [t_0,\ t_1]$: All MOSFETs are turned ON at t_0. The inductor *L* is being charged by the input voltage $V_{\rm in}$. Thus, the voltage across L, v_L, is

$$v_L(t) = V_{\rm in}. \tag{2}$$

This mode ends when all MOSFETs are turned OFF at t_1.

Mode 1, $t \in [t_1,\ t_2]$: All MOSFETs are turned OFF and all channels are activated. Thus

$$\begin{aligned} v_L(t) &= V_{\rm in} - V_{o,1} \\ &= V_{\rm in} - \sum_{i=1}^{N} V_{s,i}. \end{aligned} \tag{3}$$

This mode ends when the MOSFET Q_N is turned ON.

Mode $k, t \in [t_k,\ t_{k+1}]$, for $2 \le k \le N$: The MOSFET associated with Channel $N–k+2$ is turned ON at t_k. All LED strings from Channels 1 to $N–k+1$ are activated. Then

$$\begin{aligned} v_L(t) &= V_{\rm in} - V_{o,k} \\ &= V_{\rm in} - \sum_{i=1}^{N-k+1} V_{s,i}. \end{aligned} \tag{4}$$

This mode ends when the MOSFET associated with Channel $N–k+1$ is turned ON at t_{k+1}. In Mode N, Q_1 is turned ON at t_{N+1}, when the next switching cycle starts.

Based on (1)–(4), the inductor current i_L in Mode *k* can be expressed as

$$\begin{aligned} i_L(t) &= I_{L,k} + \frac{V_{L,k}}{L}\, t \\ &= I_{L,k} + \frac{V_{\rm in} - V_{o,k}}{L}\, t \end{aligned} \tag{5}$$

where $V_{L,k}$ is the inductor voltage in Mode $k, k = 0, 1, \ldots, N$, and $I_{L,k}$ is the initial inductor current in Mode *k*. It is noted that $V_{L,k}$ is assumed to be constant.

Based on (5), (6) is shown at the bottom of the page, where $I_{L,0}$ is the value of the inductor current at the beginning of the switching cycle and Δt_k is the duration of Mode *k*.

At steady state, the inductor current at the end of a switching cycle is the same as the one at the beginning of the next switching cycle. That is

$$I_{L,N+1} = I_{L,0}. \tag{7}$$

The average inductor current in Mode $k, \bar{I}_{L,k}$, can be expressed as

$$\bar{I}_{L,k} = \frac{I_{L,k} + I_{L,k+1}}{2}. \tag{8}$$

The energy consumed by Channel *i* in one switching cycle $E_{s,i}$ is

$$E_{s,i} = V_{s,i} \sum_{j=1}^{N-i+1} \bar{I}_{L,j}\, \Delta t_j. \tag{9}$$

The total energy consumed by all channels *E* is

$$E = \sum_{i=1}^{N} E_{s,i}. \tag{10}$$

Assume that the conversion efficiency is 100%

$$E = V_{\rm in}\, I_{\rm dc}\, T_s \tag{11}$$

where $I_{\rm dc}$ is the average input current and T_s is the switching period.

T_s can be expressed as

$$T_s = \sum_{i=0}^{N} \Delta t_i. \tag{12}$$

$$I_{L,k} = I_{L,0} + \frac{V_{\rm in}\,(\Delta t_0 + \Delta t_1 + \cdots + \Delta t_{k-1}) - V_{o,1}\,\Delta t_1 - \cdots V_{o,k-1}\,\Delta t_{k-1}}{L} \tag{6}$$

Let d_k be the duty cycle of Mode *k*

$$d_k \;=\; \frac{\Delta t_k}{T_s}. \tag{13}$$

Thus, based on (9)

$$\begin{bmatrix} E_{s,1}/V_{s,1} \\ E_{s,2}/V_{s,2} \\ \vdots \\ E_{s,k}/V_{s,k} \\ \vdots \\ E_{s,N}/V_{s,N} \end{bmatrix} = \begin{bmatrix} \overline{I}_{L,1} & \overline{I}_{L,2} & \cdots & \overline{I}_{L,k} & \cdots & \overline{I}_{L,N} \\ \overline{I}_{L,1} & \overline{I}_{L,2} & \cdots & \overline{I}_{L,k} & \cdots & 0 \\ \vdots & \vdots & \ddots & \vdots & \ddots & \vdots \\ \overline{I}_{L,1} & \overline{I}_{L,2} & \cdots & \cdots & \cdots & 0 \\ \vdots & \vdots & \ddots & \vdots & \ddots & \vdots \\ \overline{I}_{L,1} & 0 & \cdots & 0 & \cdots & 0 \end{bmatrix} \begin{bmatrix} d_1 \\ d_2 \\ \vdots \\ d_k \\ \vdots \\ d_N \end{bmatrix} T_s. \tag{14}$$

Let η_i be the luminous efficacy of the LEDs in Channel *i*. The luminous flux emitted by the LEDs in Channel i, $\phi_{s,i}$, is [28]

$$\phi_{s,i} \;=\; \eta_i \; \frac{E_{s,i}}{T_s}. \tag{15}$$

Thus, the output luminous flux, Φ_o, is

$$\begin{aligned} \Phi_o \;&=\; \sum_{i\,=\,1}^{N} \phi_{s,i} \\ &=\; \frac{1}{T_s} \; \sum_{i\,=\,1}^{N} \eta_i \; E_{s,i}. \end{aligned} \tag{16}$$

As derived in the Appendix, the ultimate CCT of the light output, CCT_o, is the function of $\phi_{s,1}, \phi_{s,2}, \ldots, \phi_{s,N}$, That is

$$\begin{aligned} \mathrm{CCT}_o \;&=\; \Im\left(\phi_{s,1},\; \phi_{s,2},\; \ldots, \phi_{s,N}\right) \\ &=\; \Im\left(\frac{\eta_1 \; E_{s,1}}{T_s},\; \frac{\eta_2 \; E_{s,2}}{T_s},\; ...,\; \frac{\eta_N \; E_{s,N}}{T_s}\right). \end{aligned} \tag{17}$$

Detailed derivation of (17) is given in the Appendix. A particular case is that all strings have the same forward voltages, i.e., $V_{s,1} = V_{s,2} = \ldots = V_{s,N}$. If the inductor *L* is sufficiently large, its current is fairly constant. Thus, $\bar{I}_{L,1} = \bar{I}_{L,2} = \ldots = \bar{I}_{L,N}$. Based on (14), CCT is purely determined by the duty cycles $d_0, d_1, \ldots, d_N$.

III. Example—Two-Channel System

A two-channel system is illustrated in this section. The first channel consists of a 7 W LED module of CCT 2700 K (warm white). The second channel consists of a 7 W LED module of CCT 5000 K (cool white). Warm and cool colors have different psychological effects [29]. With both warm and cool LED channels placed in an LED lamp, it is possible for one to adjust the color temperature of the lamp.

Fig. 3(a) shows the circuit schematic and control block diagram. Fig. 3(b) shows the key waveforms. Based on (5), (7), and (8)

$$I_{L,1} \;=\; I_{L,0} \;+\; \frac{V_{\mathrm{in}}}{L}\; \Delta t_0 \tag{18}$$

$$I_{L,2} \;=\; I_{L,1} \;+\; \frac{V_{\mathrm{in}} - V_{s,1} - V_{s,2}}{L}\; \Delta t_1 \tag{19}$$

$$I_{L,3} \;=\; I_{L,2} \;+\; \frac{V_{\mathrm{in}} \;-\; V_{s,1}}{L}\; \Delta t_2 \tag{20}$$

$$I_{L,3} \;=\; I_{L,0} \tag{21}$$

$$\overline{I}_{L,0} \;=\; \frac{I_{L,0} \;+\; I_{L,1}}{2} \tag{22}$$

$$\overline{I}_{L,1} \;=\; \frac{I_{L,1} \;+\; I_{L,2}}{2} \tag{23}$$

$$\overline{I}_{L,2} \;=\; \frac{I_{L,2} \;+\; I_{L,3}}{2}. \tag{24}$$

Based on (12) and (13)

$$T_s \;=\; \Delta t_0 \;+\; \Delta t_1 \;+\; \Delta t_2 \tag{25}$$

$$d_1 \;=\; \frac{\Delta t_1}{T_s} \tag{26}$$

$$d_2 \;=\; \frac{\Delta t_2}{T_s}. \tag{27}$$

Thus, by using (14),

$$\begin{bmatrix} E_{s,1}/V_{s,1} \\ E_{s,2}/V_{s,2} \end{bmatrix} \;=\; \begin{bmatrix} \overline{I}_{L,1} & \overline{I}_{L,2} \\ \overline{I}_{L,1} & 0 \end{bmatrix} \begin{bmatrix} d_1 \\ d_2 \end{bmatrix} \; T_s. \tag{28}$$

Based on (11),

$$E_{s,1} \;+\; E_{s,2} \;=\; V_{\mathrm{in}} \; I_{\mathrm{dc}} \; T_s. \tag{29}$$

The average input current I_{dc} is

$$I_{\mathrm{dc}} \;=\; \frac{\overline{I}_{L,0} \; \Delta t_0 \;+\; \overline{I}_{L,1} \; \Delta t_1 \;+\; \overline{I}_{L,2} \; \Delta t_2}{T_s}. \tag{30}$$

Based on (16), the output luminous flux Φ_o is

$$\Phi_o \;=\; \frac{1}{T_s} \; (\eta_1 \; E_{s,1} \;+\; \eta_2 \; E_{s,2}). \tag{31}$$

As shown in the Appendix, the CCT_o of a two-channel system depends on the ratio of the output luminous flux of the two channels

$$\mathrm{CCT}_o \;=\; \rho\left(\frac{\phi_{s,2}}{\phi_{s,1}}\right). \tag{32}$$

As defined in (15), $\phi_{s,i}$ can also be expressed as a function of the energy. CCT_o is then a function of the ratio $E_{s,2}\;/\;E_{s,1}$. In particular, the forward voltages of the two channels are the same and the current variation is relatively small in this application. CCT_o can then be expressed as a function of the ratio of the duty cycles.

It should be noted in the analysis that $E_{s,1}$ represents the energy consumed by the LED channel with the longer conduction time, while $E_{s,2}$ represents the energy consumed by the LED channel with the shorter conduction time. Thus, $E_{s,2} \leq E_{s,1}$. For example, if the conduction time of the warm LED channel

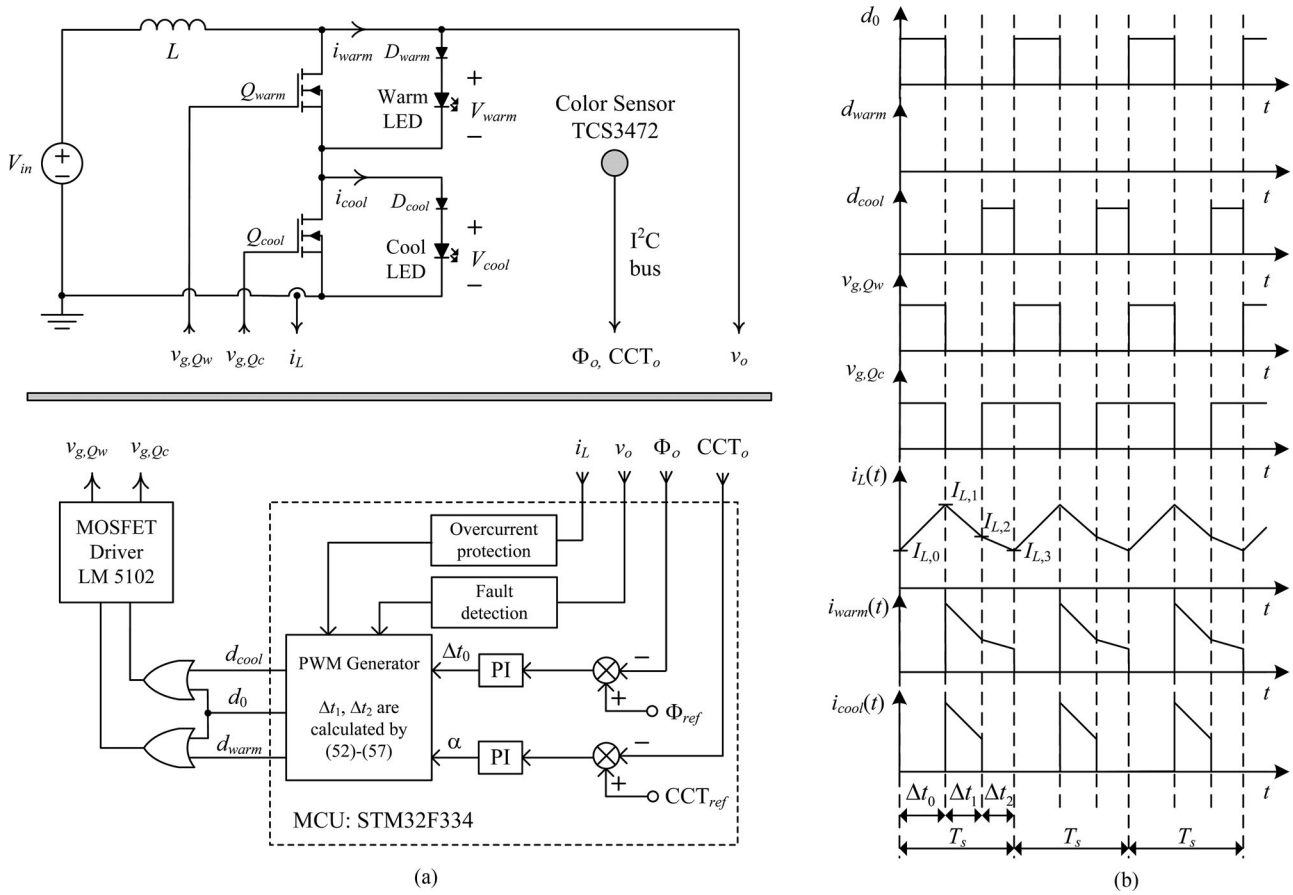

Fig. 3. Two-channel system. (a) Power stage and controller, (b) Key waveforms when the lamp operates in Scenario 1.

TABLE I
COMPONENT AND PARAMETER VALUES

Component/Parameter	Value
$V_{\rm in}$	20 V
f_s	200 kHz
L	2 mH
$D_{\rm warm}$ and $D_{\rm cool}$	LL4148
$Q_{\rm warm}$ and $Q_{\rm cool}$	IRF530N
Warm LED	CXA1507-0000-000N00E427H
Cool LED	CXA1507-0000-000N00G250H

is longer, the warm LED channel is Channel 1 and the cool LED channel is Channel 2. Then, $E_{s,1} = E_{\rm warm}$, which is the energy consumed by the warm LED channel in one switching cycle, and $E_{s,2} = E_{\rm cool}$, which is the energy consumed by the cool LED channel in one switching cycle. Conversely, if the conduction time of the cool LED channel is longer, the cool LED channel becomes Channel 1 and the warm LED channel becomes Channel 2. Then, $E_{s,1} = E_{\rm cool}$ and $E_{s,2} = E_{\rm warm}$. Fig. 4(a) shows the measured $\rm CCT_o$ versus the energy ratio, $E_{s,2}\ /\ E_{s,1}$. Fig. 4(b) shows the measured $\rm CCT_o$ versus the ratio of the duty cycles, $d_1\ /\ (d_1\ +\ d_2)$. The components used in the prototype are listed in Table I. The measurements are conducted in an integrating sphere with the spectrophotocolorimeter Everfine PMS-80.

Let

$$m\ =\ \frac{d_1}{d_1\ +\ d_2}. \tag{33}$$

The $\rm CCT_o$ is in piecewise-linear relationship with the values of $E_{s,2}\ /\ E_{s,1}$ and m. Based on the experimental results, $\rm CCT_o$ can be described by the following equations:

$$\mathrm{CCT}_o\ =\ \begin{cases} 1337.5m + 2712.83, & \text{for } E_{\rm cool} < E_{\rm warm},\ 0 \le m < 0.4 \\ 689\ m + 2975.2, & \text{for } E_{\rm cool} \le E_{\rm warm},\ 0.4 \le m \le 1 \\ -1747.5\ m + 4801.83, & \text{for } E_{\rm cool} > E_{\rm warm},\quad 0 \le m < 0.4 \\ -781.5\ m + 4407.3, & \text{for } E_{\rm cool} \ge E_{\rm warm},\ 0.4 \le m \le 1 \end{cases} \tag{34}$$

m can be approximated as the energy ratio of the two channels, that is

$$m \approx E_{s,2}/E_{s,1}. \tag{35}$$

Fig. 4 shows the curves of the functions given in (34), which are in close agreement with the experimental results. Based on

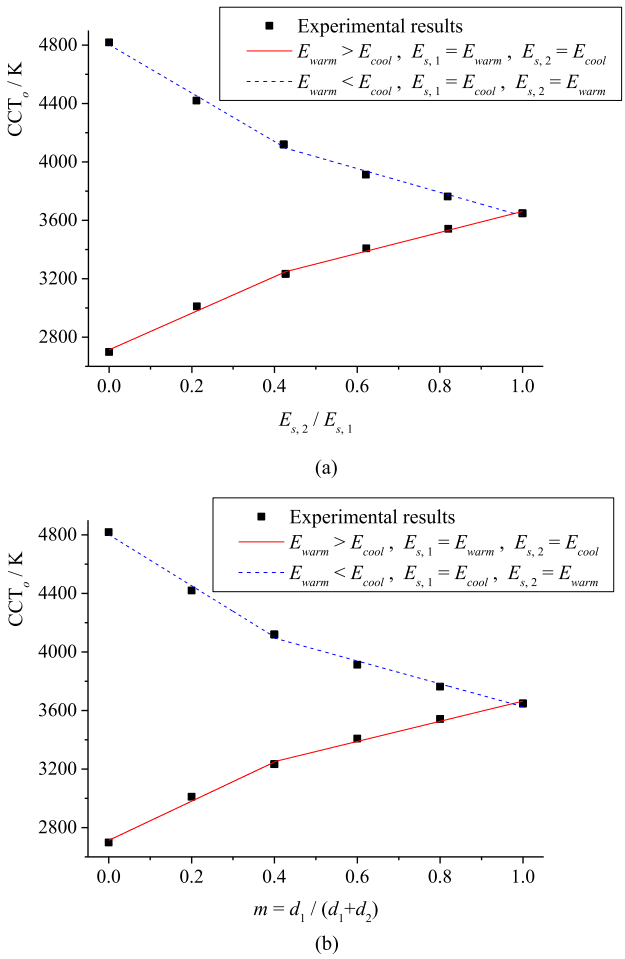

Fig. 4. Experimental results of CCT_o with varying energy ratio or varying ratio of the duty cycles of the two channels. (a) CCT_o versus $E_{s,2} \ / \ E_{s,1}$, (b) CCT_o versus m.

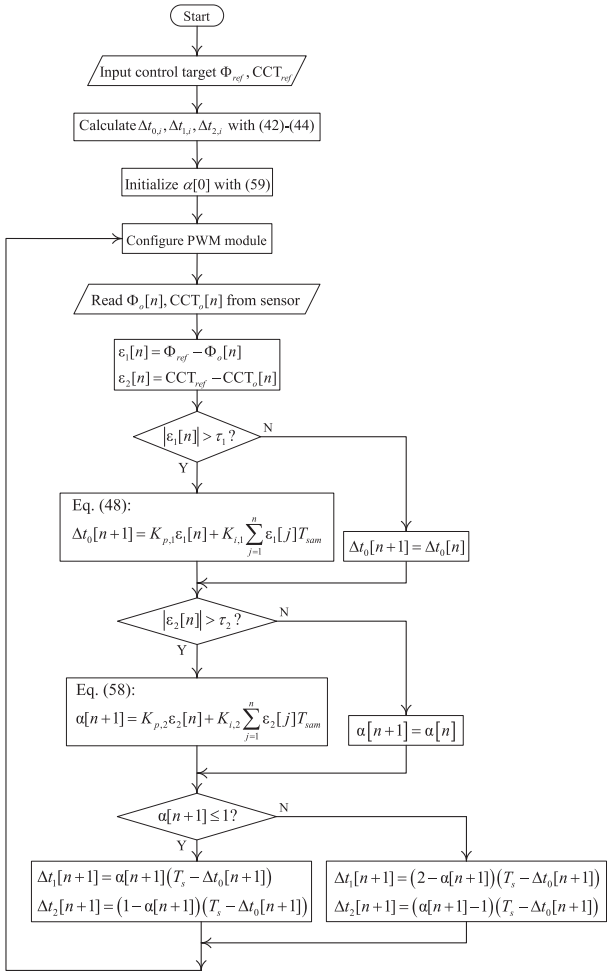

Fig. 5. Control flowchart for regulating Φ_o and CCT_o.

(34), m can be expressed as a function of CCT_o

$$m = \begin{cases} \dfrac{1}{1337.5}\,(\mathrm{CCT}_o - 2712.83), & \text{for } 2713 \le \mathrm{CCT}_o < 3250 \\ \dfrac{1}{689}(\mathrm{CCT}_o - 2975.2), & \text{for } 3250 \le \mathrm{CCT}_o < 3650 \\ -\dfrac{1}{781.5}\,(\mathrm{CCT}_o - 4407.3), & \text{for } 3650 \le \mathrm{CCT}_o < 4100 \\ -\dfrac{1}{1747.5}\,(\mathrm{CCT}_o - 4801.83), & \text{for } 4100 \le \mathrm{CCT}_o \le 4801 \end{cases}. \tag{36}$$

Φ_o and CCT_o are controlled by adjusting the time intervals $\Delta t_0, \Delta t_1$, and Δt_2. They are regulated by a feedback mechanism, as depicted in Fig. 3(a). They are measured by a color sensor and are compared with the corresponding references Φ_{ref} and $\mathrm{CCT}_{\mathrm{ref}}$, respectively. Their errors are processed by two corresponding proportional-plus-integral (PI) controllers. Based on the outputs of the PI controllers, Δt_0, Δt_1, and Δt_2 are derived by a PWM generator. Detailed operations of the PI controllers and PWM generator will be discussed in Section III-B.

To enhance the speed of regulating Φ_o and CCT_o, the initial values of $\Delta t_0, \Delta t_1$, and Δt_2 are estimated before entering the feedback control loop. The flowchart of the control mechanism is shown in Fig. 5. The procedures of the initial estimation and the mechanism of the control loop are described as follows.

A. *Initial Estimation of the Switching Times*

The initial values of $\Delta t_0, \Delta t_1$, and Δt_2, denoted by $\Delta t_{0,i}, \Delta t_{1,i}$, and $\Delta t_{2,i}$, respectively, are estimated by first determining the initial value of m, m_i, with (36) and $\mathrm{CCT}_o = \mathrm{CCT}_{\mathrm{ref}}$. $\Delta t_{1,i}$, and $\Delta t_{2,i}$ are expressed in terms of $\Delta t_{0,i}$ as

$$\Delta t_{1,i} = m_i\,(T_s - \Delta t_{0,i}) \tag{37}$$

$$\Delta t_{2,i} = (1 - m_i)\,(T_s - \Delta t_{0,i}). \tag{38}$$

Based on (29), (31), and (35)

$$E_{s,1} = \frac{T_s\ \Phi_{\mathrm{ref}}}{\eta_1 + m_i\eta_2} \tag{39}$$

$$E_{s,2} = \frac{m_i T_s\ \Phi_{\mathrm{ref}}}{\eta_1 + m_i\eta_2} \tag{40}$$

$$I_{dc} = \frac{(1 + m_i)\ \Phi_{\mathrm{ref}}}{(\eta_1 + m_i\eta_2)\ V_{\mathrm{in}}}. \tag{41}$$

By using (18)–(24), (30), (37), and (38)

$$\Delta t_{0,i} = \frac{V_{s,1} + m_i V_{s,2} - V_{\rm in}}{V_{s,1} + m_i V_{s,2}} T_s \tag{42}$$

$$\Delta t_{1,i} = \frac{m_i V_{\rm in}}{V_{s,1} + m_i V_{s,2}} T_s \tag{43}$$

$$\Delta t_{2,i} = \frac{V_{\rm in} - m_i V_{\rm in}}{V_{s,1} + m_i V_{s,2}} T_s \tag{44}$$

$$\begin{aligned} I_{L,3} = I_{L,0} = {} & \frac{1}{2L(V_{s,1} + m_i V_{s,2})^2} (T_s V_{\rm in}^2 V_{s,1} \\ & + 2 I_{\rm dc} L V_{s,1}^2 - T_s V_{\rm in} V_{s,1}^2 + 2 m_i T_s V_{\rm in}^2 V_{s,2} \\ & - m_i^2 T_s V_{\rm in}^2 V_{s,2} + 4 I_{\rm dc} m_i L V_{s,1} V_{s,2} \\ & - 2 m_i T_s V_{\rm in} V_{s,1} V_{s,2} + 2 I_{\rm dc} m_i^2 L V_{s,2}^2 \\ & - m_i^2 T_s V_{\rm in} V_{s,2}^2) \end{aligned} \tag{45}$$

$$\begin{aligned} I_{L,1} = {} & \frac{1}{2L(V_{s,1} + m_i V_{s,2})^2} (-T_s V_{\rm in}^2 V_{s,1} \\ & + 2 I_{\rm dc} L V_{s,1}^2 + T_s V_{\rm in} V_{s,1}^2 - m_i^2 T_s V_{\rm in}^2 V_{s,2} \\ & + 4 I_{\rm dc} m_i L V_{s,1} V_{s,2} + 2 m_i T_s V_{\rm in} V_{s,1} V_{s,2} \\ & + 2 I_{\rm dc} m_i^2 L V_{s,2}^2 + m_i^2 T_s V_{\rm in} V_{s,2}^2) \end{aligned} \tag{46}$$

$$\begin{aligned} I_{L,2} = {} & \frac{1}{2L(V_{s,1} + m_i V_{s,2})^2} (-T_s V_{\rm in}^2 V_{s,1} \\ & + 2 m_i T_s V_{\rm in}^2 V_{s,1} + 2 I_{\rm dc} L V_{s,1}^2 + T_s V_{\rm in} V_{s,1}^2 \\ & - 2 m_i T_s V_{\rm in} V_{s,1}^2 + m_i^2 T_s V_{\rm in}^2 V_{s,2} \\ & + 4 I_{\rm dc} m_i L V_{s,1} V_{s,2} - 2 m_i^2 T_s V_{\rm in} V_{s,1} V_{s,2} \\ & + 2 I_{\rm dc} m_i^2 L V_{s,2}^2 - m_i^2 T_s V_{\rm in} V_{s,2}^2). \end{aligned} \tag{47}$$

Thus, $\Delta t_{0,i}, \Delta t_{1,i}$, and $\Delta t_{2,i}$ given in (42)–(44) are used in the initial setting. A more accurate estimation can be done with the channel voltages being calculated with an approximate linear model for LED [30].

B. Feedback Control Mechanism

Φ_o and CCT_o are regulated at $\Phi_{\rm ref}$ and $\mathrm{CCT}_{\rm ref}$, respectively, by using two control loops. The first loop generates Δt_0 by using the error between Φ_o and $\Phi_{\rm ref}$, i.e., ε_1. Fig. 6(a) shows the measured Φ_o and CCT_o versus Δt_0 with $m = 0.2, 0.6$, and 1.0, respectively, when $E_{\rm cool} \le E_{\rm warm}$. With m fixed, Φ_o varies with Δt_0 while CCT_o is relatively constant. With the increase in the inductor charging time interval Δt_0, the average inductor current and Φ_o increase. CCT_o is relatively constant, as it is determined by the flux ratio described in (32). Fig. 6(b) shows the measured Φ_o and CCT_o versus Δt_0 with $m = 0.2, 0.6$, and 1.0, respectively, when $E_{\rm cool} \ge E_{\rm warm}$. Similar characteristics as in Fig. 6(a) are observed.

Thus, the first digital PI control is defined as

$$\Delta t_0[n+1] = K_{p,1}\varepsilon_1[n] + K_{i,1}\sum_{j=1}^{n}\varepsilon_1[j]T_{\rm sam} \tag{48}$$

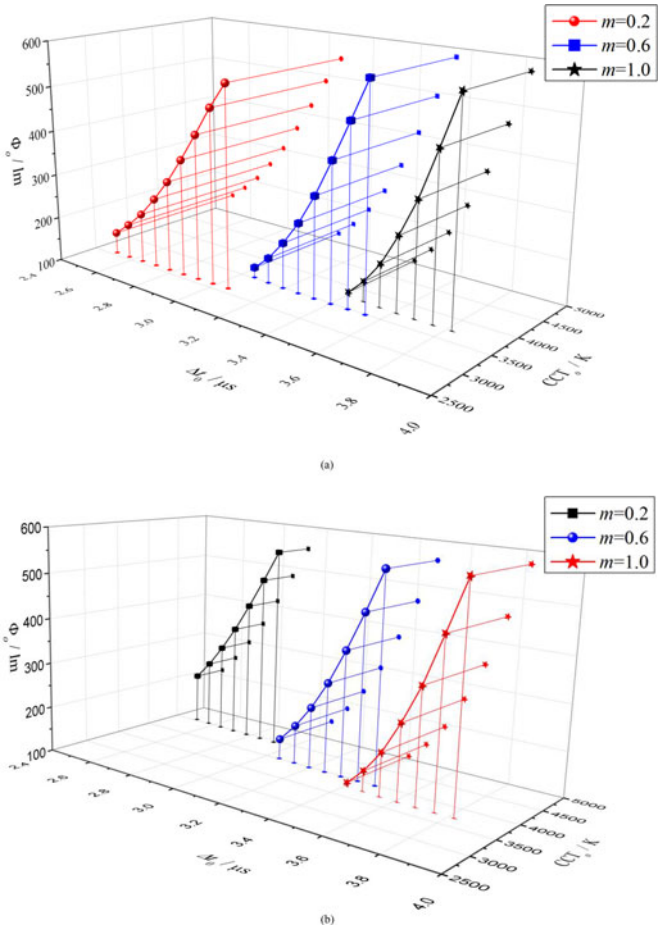

Fig. 6. Measured Φ_o and CCT_o versus Δt_0 with different values of m. (a) $E_{\rm cool} \le E_{\rm warm}$, (b) $E_{\rm cool} \ge E_{\rm warm}$.

where $\Delta t_0[n+1]$ is the value of Δt_0 used in the $(n+1)$th sample, $\varepsilon_1[j] = \Phi_{\rm ref} - \Phi_o[j]$, $\Phi_o[j]$ is the jth sample of Φ_o, $K_{p,1}$ is the proportional gain, and $K_{i,1}$ is the integral gain, $T_{\rm sam}$ is the sampling time period.

The second loop generates Δt_1 and Δt_2 by using the error $\varepsilon_2 = \mathrm{CCT}_{ref} - \mathrm{CCT}_o$, and

$$\Delta t_1 + \Delta t_2 = T_s - \Delta t_0. \tag{49}$$

Based on (33)

$$\Delta t_1 = m(T_s - \Delta t_0). \tag{50}$$

As Δt_0 is generated in the first loop, Δt_1 is determined by m. As shown in (34), the value of m overlaps under the whole operating conditions. A variable α is used to transform the value of m to define the operating condition. Fig. 7(a) shows the transformation function. The value of α varies between 0 and 2. It is defined as

$$\alpha = \begin{cases} m, & \text{for } E_{\rm cool} < E_{\rm warm} \\ 2 - m, & \text{for } E_{\rm cool} > E_{\rm warm} \end{cases}. \tag{51}$$

Equation (33) shows that m, the ratio of the duty cycles, is a key parameter in the electrical analysis. α is the variable de-

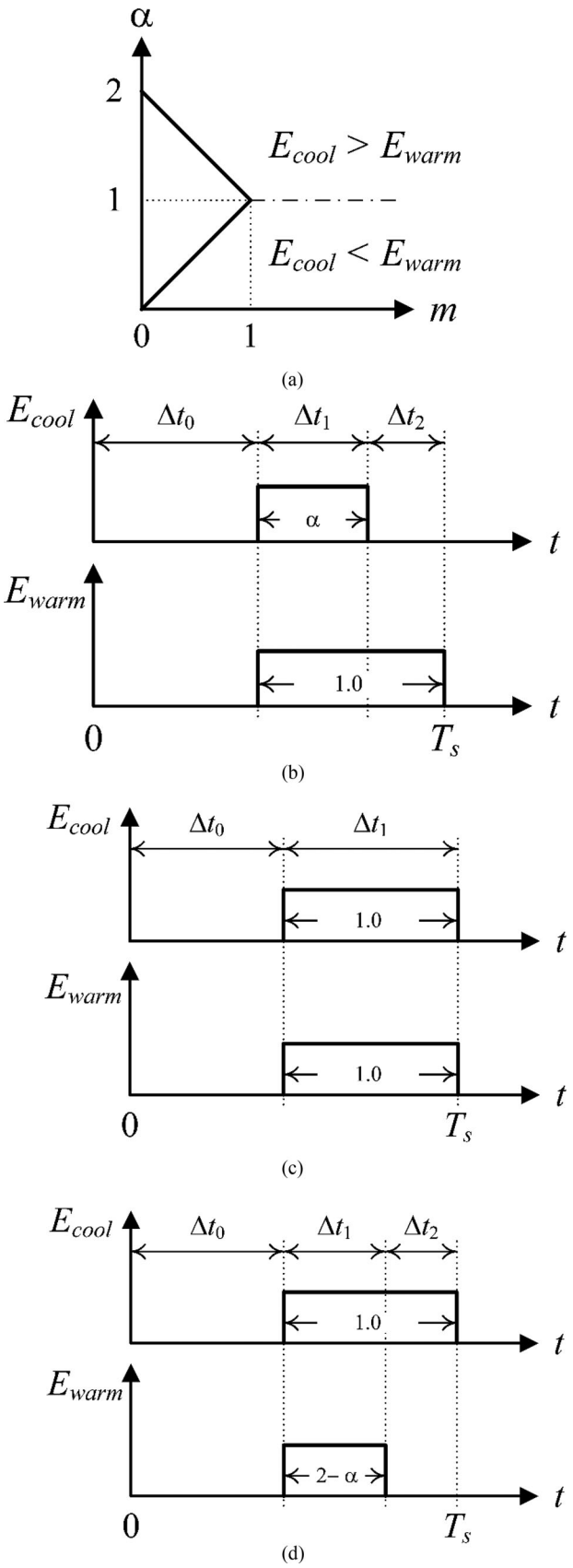

Fig. 7. Relationship between α and m, and three operating scenarios. (a) Relationship between α and m, (b) Scenario 1: $E_{\rm cool} < E_{\rm warm}$, $0 \le \alpha < 1.0$, and $m = \alpha$, (c) Scenario 2: $E_{\rm cool} = E_{\rm warm}$, and $m = \alpha = 1$, (d) Scenario 3: $E_{\rm cool} > E_{\rm warm}$, $1 < \alpha \le 2$, and $m = 2 - \alpha$.

termining the operating scenarios shown in Fig. 7. Thus, (51) shows that α bridges the electrical analysis and the optical characteristics. Based on (51), there are three possible scenarios as illustrated in Fig. 7.

Scenario 1: As illustrated in Fig. 7(b), $0 \le \alpha < 1$, $E_{\rm cool} < E_{\rm warm}$, the conduction time of the warm LED channel is longer, so the warm LED channel is Channel 1 and the cool LED channel is Channel 2

$$\Delta t_1 \;=\; \alpha\,(T_s \;-\; \Delta t_0) \tag{52}$$

and

$$\Delta t_2 \;=\; (1-\alpha)\,(T_s \;-\; \Delta t_0)\,. \tag{53}$$

The key voltage and current waveforms in this scenario are given in Fig. 3(b).

Scenario 2: As illustrated in Fig. 7(c), $\alpha = 1$, $E_{\rm cool} = E_{\rm warm}$, the conduction time of the warm LED channel is the same as that of the cool LED. Then, the warm LED channel can be Channel 1 or Channel 2, and the cool LED channel can be Channel 2 or Channel 1, respectively

$$\Delta t_1 \;=\; T_s \;-\; \Delta t_0 \tag{54}$$

$$\Delta t_2 \;=\; 0. \tag{55}$$

Scenario 3: As illustrated in Fig. 7(d), $1 < \alpha \le 2$, $E_{\rm cool} > E_{\rm warm}$, the conduction time of the cool LED channel is longer, so the cool LED channel is Channel 1 and the warm LED channel is Channel 2

$$\Delta t_1 \;=\; (2-\alpha)\,(T_s \;-\; \Delta t_0) \tag{56}$$

and

$$\Delta t_2 \;=\; (\alpha-1)(T_s \;-\; \Delta t_0). \tag{57}$$

The voltage and current waveforms in this scenario are similar to that in Scenario 1, except that the corresponding waveforms associated with the warm LED channel and cool LED channel are interchanged.

Based on (52)–(57), α is the generated parameter in the second loop through the other digital PI controller with the control law of

$$\alpha[n+1] = K_{p,2}\varepsilon_2[n] + K_{i,2}\sum_{j=1}^{n}\varepsilon_2[j]T_{\rm sam} \tag{58}$$

where $\alpha[n+1]$ is the value of α generated in the $(n+1)$th sample, $\varepsilon_2[j] = {\rm CCT}_{\rm ref} - {\rm CCT}_o[j]$, ${\rm CCT}_o[j]$ is the jth sample of ${\rm CCT}_o$, $K_{p,2}$ is the proportional gain, and $K_{i,2}$ is the integral gain, $T_{\rm sam}$ is the sampling time period. As for the initial value of α, $\alpha[0]$, after m_i is calculated with (36), $\alpha[0]$ can be calculated based on (51) by

$$\alpha[0] \;=\; \begin{cases} m_i, & \text{for } 2713 \;\le {\rm CCT}_{\rm ref} < 3650 \\ 2 \;-\; m_i, & \text{for } \;3650 \le {\rm CCT}_{\rm ref} \le 4801 \end{cases}. \tag{59}$$

The two control loops give the updated values of Δt_0 and α, i.e., $\Delta t_0[n+1]$ and $\alpha[n+1]$, respectively. $\Delta t_1[n+1]$ and $\Delta t_2[n+1]$ can be calculated with (52)–(57). The duty cycle value of PWM signal d_0, $d_{\rm warm}$, and $d_{\rm cool}$, shown in Fig. 3, in

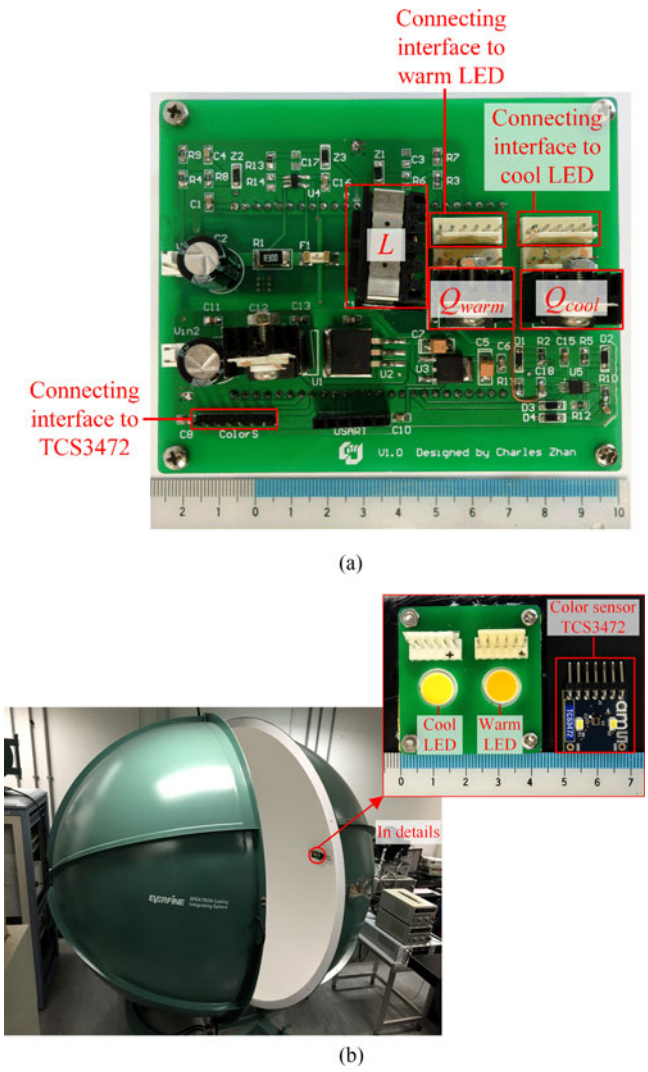

Fig. 8. Hardware implementation and testing. (a) Prototype. (b) Testing setup.

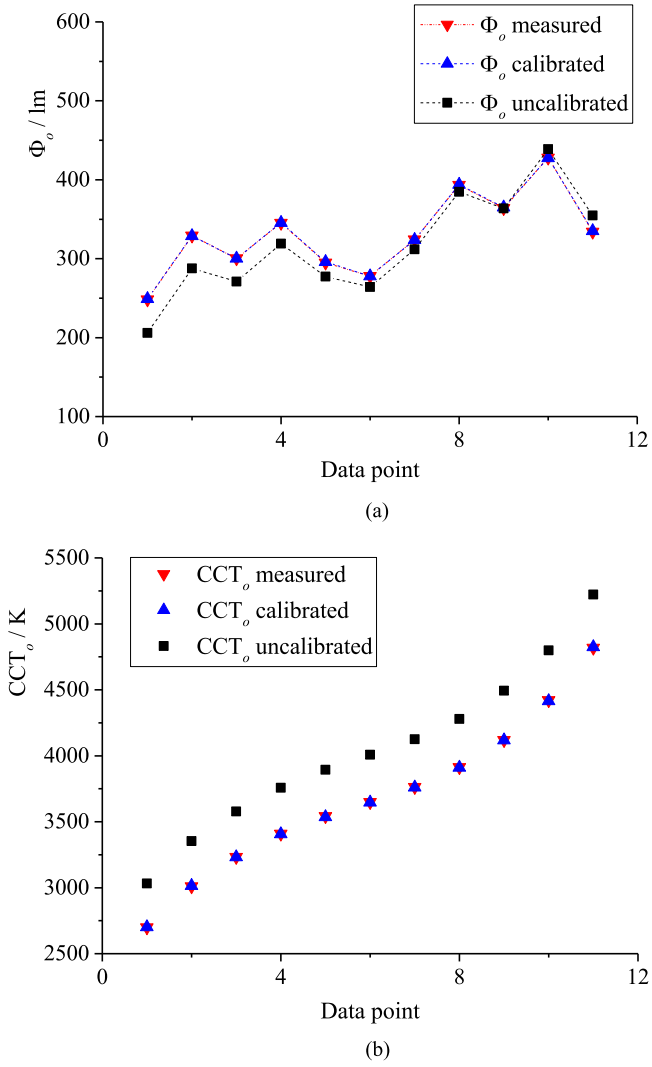

Fig. 9. Comparisons of Φ_o and CCT_o measured by the spectrophotocolorimeter system, by the color sensor before and after calibration. (a) Comparison of Φ_o. (b) Comparison of CCT_o.

$(n+1)$th sample, i.e., $d_0[n+1]$, $d_{\mathrm{warm}}[n+1]$, and $d_{\mathrm{cool}}[n+1]$, can be configured by using $\alpha[n+1]$, $\Delta t_0[n+1]$, $\Delta t_1[n+1]$, and $\Delta t_2[n+1]$, as illustrated in Figs. 3 and 7(b)–(d)

$$d_0[n+1] = \frac{\Delta t_0[n+1]}{T_s}. \tag{60}$$

If $0 \le \alpha[n+1] < 1$, the operation is in Scenario 1,

$$d_{\mathrm{warm}}[n+1] = 0 \tag{61}$$

and

$$d_{\mathrm{cool}}[n+1] = d_2[n+1] = \frac{\Delta t_2[n+1]}{T_s}. \tag{62}$$

If $\alpha[n+1] = 1$, the operation is in Scenario 2

$$d_{\mathrm{warm}}[n+1] = 0 \tag{63}$$

and

$$d_{\mathrm{cool}}[n+1] = 0. \tag{64}$$

If $1 < \alpha[n+1] \le 2$, the operation is in Scenario 3,

$$d_{\mathrm{warm}}[n+1] = d_2[n+1] = \frac{\Delta t_2[n+1]}{T_s} \tag{65}$$

and

$$d_{\mathrm{cool}}[n+1] = 0. \tag{66}$$

The timing is achieved by relative settings of different PWM channels associated with the same timer in the MCU.

IV. Experimental Verifications

A two-channel system, as described in Section III, has been built and evaluated. Its circuit schematic is shown in Fig. 3(a). Fig. 8 shows the picture of the prototype and testing setup. The parameters of the components are listed in Table I. The output luminous flux and CCT are measured by a color sensor TAOS TCS3472 [31]. They are also verified by Everfine PMS-80 spectrophotocolorimeter with an integrating sphere. The microcon-

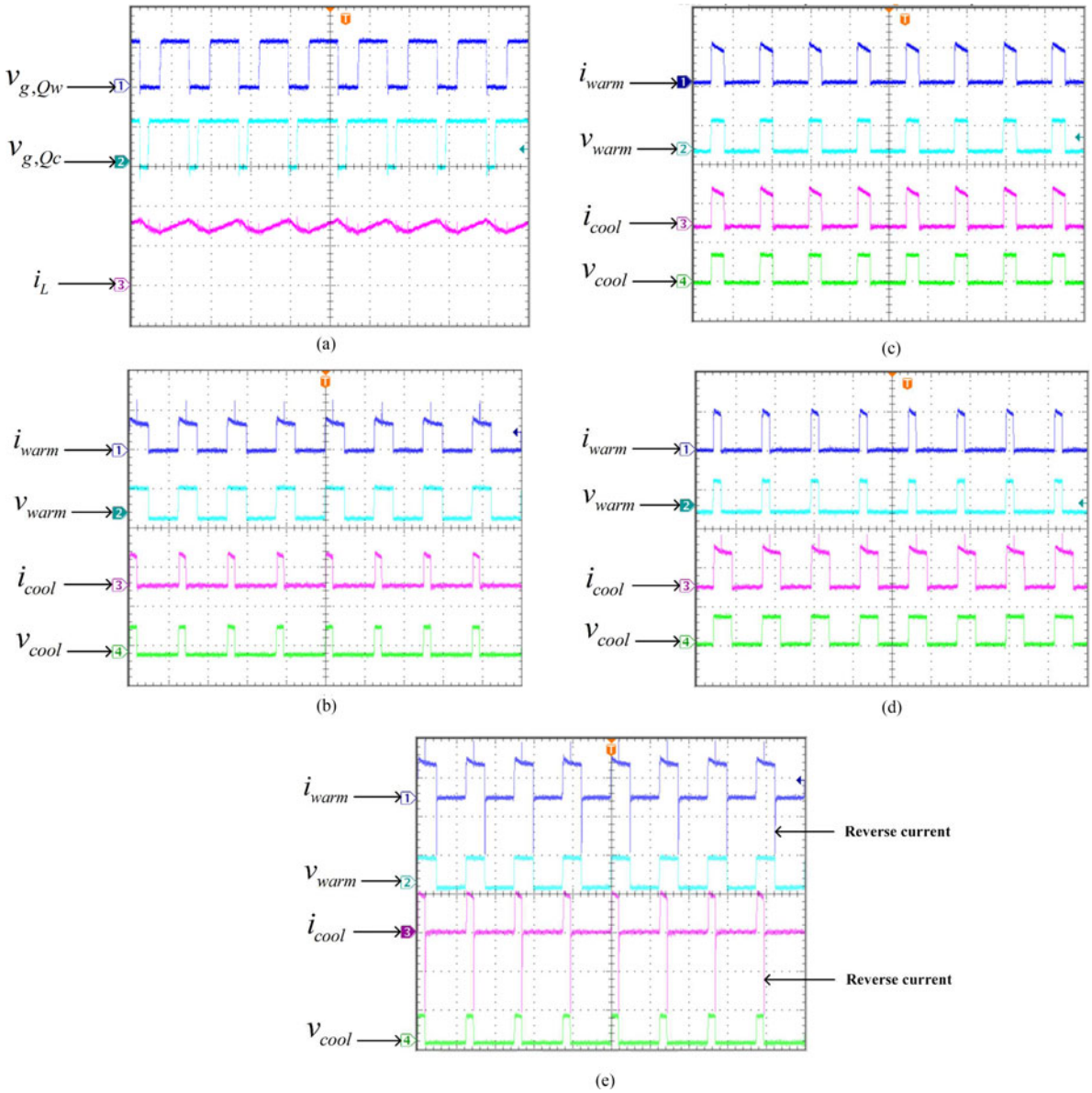

Fig. 10. Experimental waveforms of the two-channel system. (a) MOSFET driving signals, $v_{g,Qw}$ and $v_{g,Qc}$, and inductor current i_L when the lamp is operated in Scenario 1 (Ch1: $v_{g,Qw}$ (10V/div), Ch2: $v_{g,Qc}$ (10 V/div), Ch3: i_L (100 mA/div), Timebase: 4s/div), (b) LED channel currents, $i_{\rm warm}$ and $i_{\rm cool}$, and voltages, $v_{\rm warm}$ and $v_{\rm cool}$, when the lamp is operated in Scenario 1 (Ch1: $i_{\rm warm}$ (200 mA/div), Ch2: $v_{\rm warm}$ (50 V/div), Ch3: $i_{\rm cool}$ (200 mA/div), Ch4: $v_{\rm cool}$ (50 V/div), Timebase: $4\mu{\rm s/div}$), (c) LED channel currents, $i_{\rm warm}$ and $i_{\rm cool}$, and voltages, $v_{\rm warm}$ and $v_{\rm cool}$, when the lamp is operated in Scenario 2 (Ch1: $i_{\rm warm}$ (200 mA/div), Ch2: $v_{\rm warm}$ (50 V/div), Ch3: $i_{\rm cool}$ (200 mA/div), Ch4: $v_{\rm cool}$ (50 V/div), Timebase: $4\mu{\rm s/div}$), (d) LED channel currents, $i_{\rm warm}$ and $i_{\rm cool}$, and voltages, $v_{\rm warm}$ and $v_{\rm cool}$, when the lamp is operated in Scenario 3 (Ch1: $i_{\rm warm}$ (200 mA/div), Ch2: $v_{\rm warm}$ (50 V/div), Ch3: $i_{\rm cool}$ (200 mA/div), Ch4: $v_{\rm cool}$ (50 V/div), Timebase: $4\mu{\rm s/div}$), (e) LED channel currents, $i_{\rm warm}$ and $i_{\rm cool}$, and voltages, $v_{\rm warm}$ and $v_{\rm cool}$, when the lamp is operated in Scenario 1 without the series-connected diodes (Ch1: $i_{\rm warm}$ (200 mA/div), Ch2: $v_{\rm warm}$ (50 V/div), Ch3: $i_{\rm cool}$ (200 mA/div), Ch4: $v_{\rm cool}$ (50 V/div), Timebase: $4\mu{\rm s/div}$).

troller STM32F334 first reads the red, green, blue, and clear light sensing values from the color sensor via an I^2C bus. Then, Φ_o and $\rm CCT_o$ are calculated, according to [32], which are also calibrated by the spectrophotocolorimeter system. The stability of the entire control system is assured. Detailed mathematical treatments are given in the Appendix.

Fig. 9 shows the comparison of Φ_o and $\rm CCT_o$, in which "Φ_o measured" and "$\rm CCT_o$ measured" are the data measured by the spectrophotocolorimeter system, "Φ_o calibrated" and "$\rm CCT_o$ calibrated" are the data after calibration, and "Φ_o uncalibrated" and "$\rm CCT_o$ uncalibrated" are the data before calibration. They are obtained by the method described in [32]. The uncalibrated data obtained by the color sensor does not well match with the data obtained by spectrophotocolorimeter. After calibration, the data obtained by the color sensor can match well with the one measured by the spectrophotocolorimeter.

The control algorithm shown in Fig. 5 has been implemented. The feedback mechanism in the control loops relies on the information from the color sensor without sensing the inductor current or channel current. The sensed inductor current i_L, shown in Fig. 3(a), is only used for the overcurrent protection.

For driving the two MOSFETs, the gate driver Texas Instruments LM5102 is used. It is designed to drive both the high- and low-side MOSFETs. The outputs can be controlled

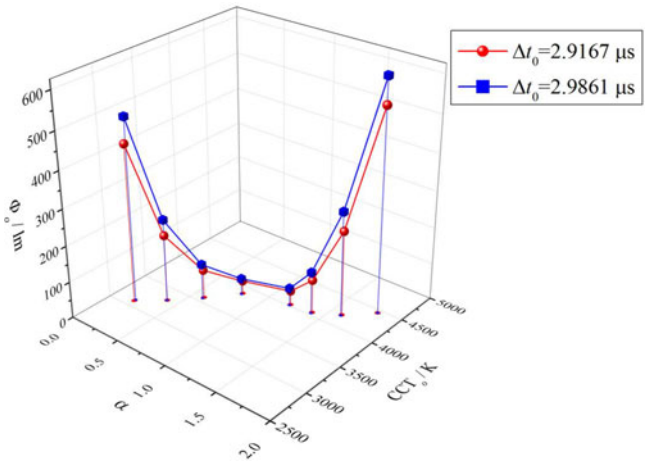

Fig. 11. Measured Φ_o and CCT_o versus α with constant Δt_0.

independently. That is, driving the MOSFET associated with an LED channel does not affect the driving of MOSFET associated with the other LED channel. As both MOSFETs are turned ON for charging the inductor at the beginning of each switching cycle, the bootstrap capacitor in the gate driver will be charged up in every switching cycle.

The waveforms of MOSFET gate signals, inductor current in Scenario 1, LED currents and voltages in Scenarios 1, 2, 3 are shown in Fig. 10(a)–(d). The waveforms are in close agreement with the theoretical waveforms shown in Fig. 3(b). For the sake of comparison, the waveforms of the LED current and voltage in Scenario 1 without the series-connected diodes, i.e., D_{warm} and D_{cool} in Fig. 3(a), are shown in Fig. 10(e). Reverse currents appear in both warm and cool LED channels upon turning on the parallel switches. The peak reverse current of the warm LED is around 300 mA, while the peak reverse current of the cool LED is around 400 mA. Compared with the corresponding waveforms in Fig. 10(b), it can be observed that the series-connected diodes can effectively eliminate reverse current pulses. Such phenomenon can be explained by considering that a current path is created after the parallel switch is turned ON. Without the series-connected diode, the effective capacitance in the current path is the junction capacitance of the LED channels. With the series-connected diode, the effective capacitance in the current path is dominated by the capacitance of the diode. Since the junction capacitance of the series-connected diode is much smaller than that of the LEDs. Upon turning on the parallel switch, reverse current is limited by the series-connected diode because the displacement current through a capacitor is dependent on the value of the capacitance and the rate of change of the voltage across the switch. With the same voltage change, the reverse current is smaller in the case with small capacitance, that is, in the situation with the series-connected diode.

Fig. 11 shows the measured Φ_o and CCT_o versus α with constant Δt_0. When Δt_0 is fixed, variation of α will change the conduction times of the two LED channels, affecting the discharging rate of the inductor current. Thus, the average value of the inductor current and the luminous flux will be changed. When α is close to 1, the discharging rate of the inductor current will become steeper, causing decreases of the average inductor current and Φ_o. Details are described in Section V.

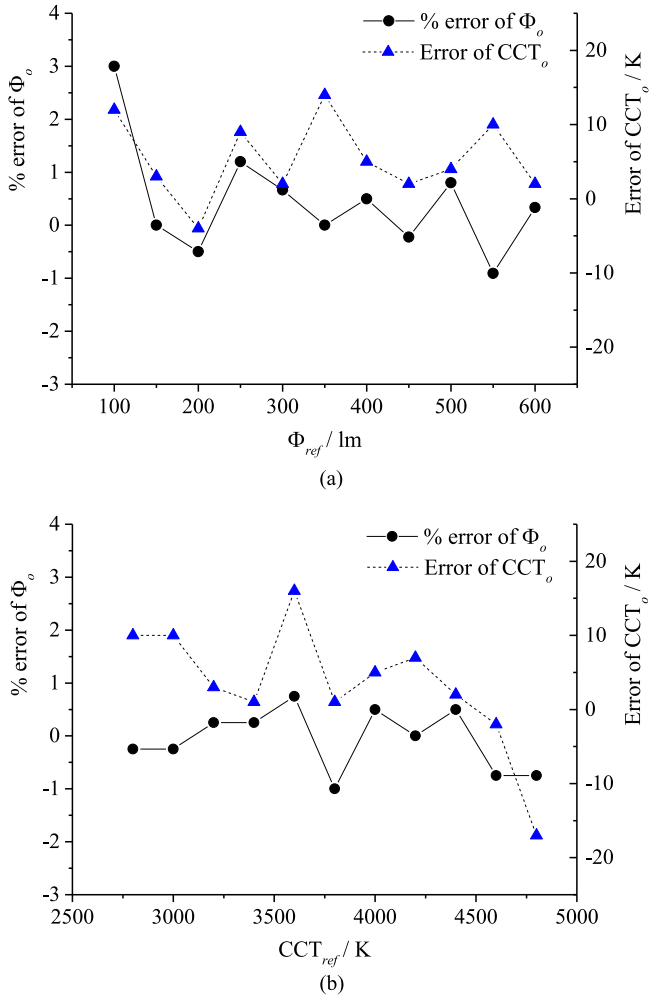

Fig. 12. Steady-state performance of the luminous flux and CCT control. (a) Steady-state error of Φ_o and CCT_o with Φ_{ref} varying between 100 and 600 lm, and $\mathrm{CCT}_{\mathrm{ref}} = 4000\mathrm{K}$, (b) Steady-state error of Φ_o and CCT_o with $\mathrm{CCT}_{\mathrm{ref}}$ varying between 2800 and 4800 K, and $\Phi_{\mathrm{ref}} = 400$ lm.

Experimental results also verify the effectiveness of the proposed control method. Fig. 12(a) shows the percentage error of Φ_o and the error of CCT_o with Φ_{ref} varying between 100 and 600 lm. As the efficacy of the LEDs is around 95.8 lm/W and the lamp power is 7 W, the maximum output is $95.8 \times 7 = 670.6\mathrm{lm}$. By considering the performance tolerance of the LEDs and losses of the driver, the maximum output is set at 600 lm. Moreover, if the lamp is allowed to dim to 20%, the minimum output is set at 100 lm.

Fig. 12(b) shows the results with $\mathrm{CCT}_{\mathrm{ref}}$ varying between 2800 and 4800 K. It was found that the CCT of the warm LED used in the prototype over the driving range varies between 2698 and 2735 K, while the CCT of the cool LED used in the prototype over the driving range varies between 4801 and 4828 K. $\mathrm{CCT}_{\mathrm{ref}}$ is set in step of 100 K. Thus, $\mathrm{CCT}_{\mathrm{ref}}$ varies between 2800 and 4800 K. The steady-state percentage error of Φ_o is around $\pm 1\%$ with a maximum of 3% at the lowest output luminous flux of 100 lm. The steady-state errors of CCT_o are within ± 20 K in both

TABLE II
STEADY-STATE ERROR OF Φ_o WITH $\mathrm{CCT}_{\mathrm{ref}} = 4000\mathrm{K}$

Φ_{ref} (lm)	Error of Φ_o (lm)	Percentage error of Φ_o (%)
100	3	3.00
150	0	0.00
200	–1	–0.50
250	3	1.20
300	2	0.67
350	0	0.00
400	2	0.50
450	–1	–0.22
500	4	0.80
550	–5	–0.91
600	2	0.33

TABLE III
STEADY-STATE ERROR OF CCTo WITH $\mathrm{CCT}_{\mathrm{ref}} = 4000$ K

Φ_{ref} (lm)	Target CCT and tolerance (K)	Error of CCT_o (K)
100	3985 ± 275	12
150	3985 ± 275	3
200	3985 ± 275	–4
250	3985 ± 275	9
300	3985 ± 275	2
350	3985 ± 275	14
400	3985 ± 275	5
450	3985 ± 275	2
500	3985 ± 275	4
550	3985 ± 275	10
600	3985 ± 275	2

TABLE IV
STEADY-STATE ERROR OF Φ_o WITH $\Phi_{\mathrm{ref}} = 400\mathrm{lm}$

$\mathrm{CCT}_{\mathrm{ref}}$ (K)	Error of Φ_o (lm)	Percentage error of Φ_o (%)
2800	–1	–0.25
3000	–1	–0.25
3200	1	0.25
3400	1	0.25
3600	3	0.75
3800	–4	–1.00
4000	2	0.50
4200	0	0.00
4400	2	0.50
4600	–3	–0.75
4800	–3	–0.75

tests. Thus, the results show that the proposed control method has a good steady-state response.

The error and percentage errors of Φ_o with Φ_{ref} varying between 100 and 600 lm and $\mathrm{CCT}_{\mathrm{ref}} = 4000\mathrm{K}$ are given in Table II. Φ_o has errors within ± 5 lm and percentage error around $\pm 1\%$ with the maximum of 3% at the lowest output of 100 lm. Thus, the steady-state performance with varying Φ_{ref} is acceptable. Table III shows that the errors of CCT_o with Φ_{ref} varying between 100 and 600 lm are very small compared with the allowable tolerance. The error and percentage errors of Φ_o with $\mathrm{CCT}_{\mathrm{ref}}$ varying between 2800 and 4800 K and $\Phi_{\mathrm{ref}} = 400\ \mathrm{lm}$ are given in Table IV. The steady-state percentage error of Φ_o is within $\pm 1\%$, which is also acceptable in practice.

TABLE V
STEADY-STATE ERROR OF CCT_o WITH $\Phi_{\mathrm{ref}} = 400$ LM

$\mathrm{CCT}_{\mathrm{ref}}$ (K)	Target CCT and tolerance (K)	Error of CCT_o (K)
2800	2800 ± 156	10
3000	3045 ± 175	10
3200	3200 ± 201	3
3400	3400 ± 218	1
3600	3600 ± 233	16
3800	3800 ± 245	1
4000	3985 ± 275	5
4200	4200 ± 267	7
4400	4400 ± 277	2
4600	4600 ± 287	–2
4800	4800 ± 298	-17

According to [33], for nominal CCTs 3000 and 4000 K, the target CCTs and tolerances are 3045±175 and 3985±275 K, respectively. For other nominal values of CCT, denoted as T, ranging from 2800 to 4800 K in step of 100 K (i.e., 2800, 2900, . . . , 4800 K), excluding 3000 and 4000 K mentioned before, the tolerance ΔT is calculated by

$$\Delta T = 1.1900 \times 10^{-8}\, T^3 - 1.5434 \times 10^{-4}\, T^2 + 0.7168\, T - 902.55. \quad (67)$$

The errors of CCT_o with comparison to the tolerances given by the above standard are shown in Table V. The errors of CCT_o with varying $\mathrm{CCT}_{\mathrm{ref}}$ are very small, as compared with the allowable tolerances. Physically speaking, the results reveal that the lamp can maintain the color temperature at any brightness or maintain the brightness at any color temperature.

Fig. 13(a) shows the transient response when Φ_{ref} is suddenly changed from 200 to 400 lm. Fig. 13(b) shows the transient response when $\mathrm{CCT}_{\mathrm{ref}}$ is suddenly changed from 3000 to 4000 K. The output can revert to the steady state in four sampling time steps, demonstrating good dynamic response.

V DISCUSSIONS

The proposed driver is basically a boost-derived converter with the output voltage being higher than the input voltage. As shown in [34], the required inductor value for a boost converter can be approximated by the equation of

$$L = \frac{V_{\mathrm{in}}\,(V_{\mathrm{out}} - V_{\mathrm{in}})}{\Delta I_L\ f_s\ V_{\mathrm{out}}} = \frac{V_{\mathrm{in}}}{\Delta I_L\ f_s}\,(1 - \frac{V_{\mathrm{in}}}{V_{\mathrm{out}}}) \quad (68)$$

where V_{out} is the average output voltage and ΔI_L is the peak-to-peak inductor ripple current.

By substituting the values given in Table I into (68), the relationships between the value of L and V_{out} with ΔI_L equal 0.01, 0.03, and 0.05 A are shown in Fig. 14. The value of the inductor does not increase linearly with the increase in V_{out}. Conversely, the value of the inductor will converge to a value depending on the inductor ripple current. This implies that the application of the proposed driver is theoretically not limited by the number of series-connected LED channels. Such condition gives a favorable condition for series-connected LED channels. Nevertheless, apart from the required value, the physical size

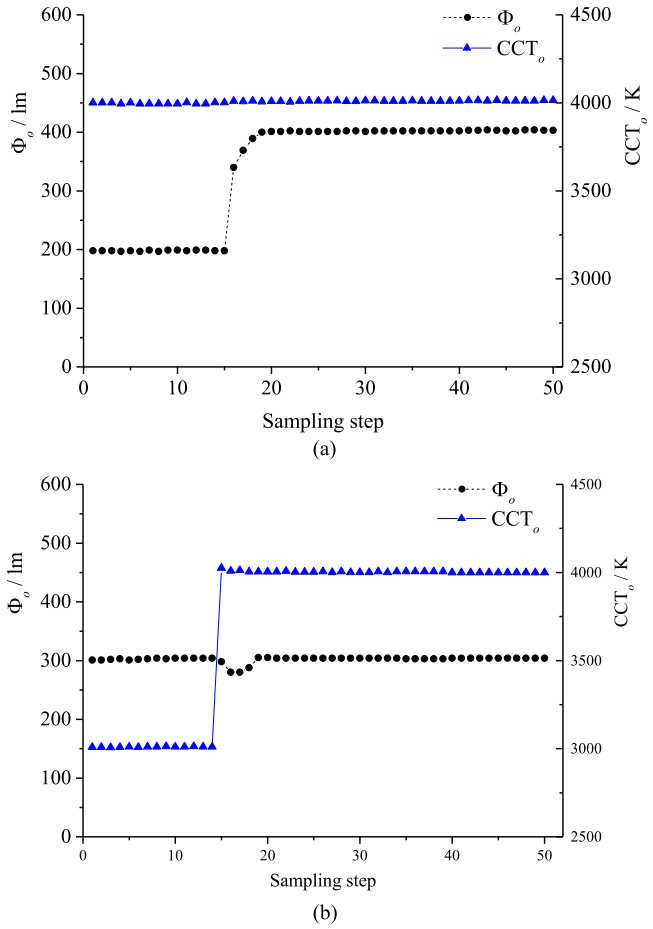

Fig. 13. Transient performance of the luminous flux and CCT control. (a) Transient response when $\Phi_{\rm ref}$ is changed from 200 to 400 lm and $\rm CCT_{ref} = 4000K$, (b) Transient response when $\rm CCT_{ref}$ is changed from 3000 to 4000 K and $\Phi_{\rm ref} = 300$ lm.

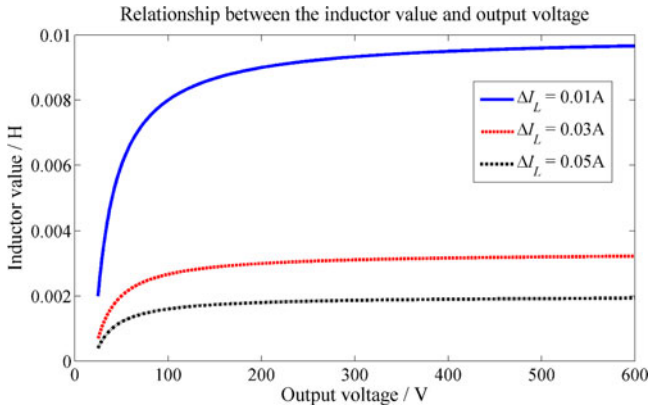

Fig. 14. Relationship between the inductor value and the output voltage.

of the inductor is also dependent on its current rating, core size selection, and loss consideration.

When Δt_0 is fixed, variation of α will change the conduction times of the two LED channels, affecting the discharging rate of the inductor current. Thus, the average value of the inductor current and the luminous flux will be changed. Fig. 15 illustrates the variation of the inductor current, when α is changed from

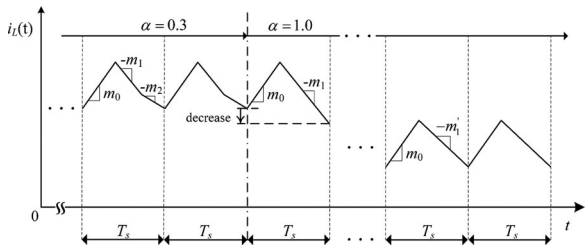

Fig. 15. Inductor current waveform when α is changed from 0.3 to 1.0 (Δt_0 is fixed).

0.3 to 1.0. For $\alpha = 0.3$, in Mode 0, both MOSFETs are turned ON and the inductor is charged. Thus, the rate of change of the inductor current is

$$m_0 = \frac{V_{\rm in}}{L}. \tag{69}$$

In Mode 1, both MOSFETs are tuned OFF and the two LED channels are activated. The output voltage

$$V_o = V_{s,1} + V_{s,2}. \tag{70}$$

Thus, the rate of change of the inductor current is

$$-m_1 = \frac{V_{\rm in} - V_{s,1} - V_{s,2}}{L}. \tag{71}$$

In Mode 2, the MOSFET across the LED channel 2 is turned ON. The output voltage is

$$V_o = V_{s,1}. \tag{72}$$

Thus, the rate of change of the inductor current is

$$-m_2 = \frac{V_{\rm in} - V_{s,1}}{L}. \tag{73}$$

By comparing (71) with (73)

$$m_1 > m_2. \tag{74}$$

With Δt_0 fixed and α changed to 1.0, the rate of change of the inductor current is $-m_1$ during the inductor discharging time ($T_s - \Delta t_0$). Since $m_1 > m_2$, the average value of i_L will reduce, as compared to the previous switching cycle. As i_L reduces, the LED forward voltage, and thus the value of m_1, will also reduce. Finally, i_L will settle to a smaller value.

Since the proposed structure has MOSFETs connected in series, the conduction loss is comparatively higher than the conduction loss of the parallel-connected structure, such as in [10]–[14]. However, such conduction loss is very small, as compared to the LED power. Consider a tetra-color system. The worst-case scenario is that only one LED channel is activated and the rest of three channels are bypassed by the three MOSFETs. Assume that the LED has the maximum forward current of 0.375 A and forward voltage of 37 V, and the on-resistance of the MOSFETs is 0.09 Ω, which are based on the parameters of the components used in the experimental prototype. The conduction loss of the three MOSFETs is $0.375^2 \times 0.09 \times 3\rm W = 0.038W$. The power of the activated LED channel is $0.375 \times 37\rm W = 13.875W$. Thus, the percentage of the MOSFET conduction loss, as compared with the LED

TABLE VI
COMPARISONS OF THE PROPOSED DRIVER WITH OTHER STATE-OF-ART DRIVERS

Parameter	SIMO driver with parallel-connected channels	Driver in [27]	Proposed driver
Number of power switches	$1+N$	$2+N$	N
Number of inductor	1	1	1
Sensitive to channel switching?	Yes	No	No
Concurrent driving?	No	Yes	Yes
Requirement for $V_{\rm in}$	$V_{\rm in} > V_o$ or $V_{\rm in} < V_o$	$V_{\rm in} > V_o$	$V_{\rm in} < V_o$

power is $(0.038/13.875) \times 100\% = 0.27\%$, which is small and acceptable in practice. The percentage will be reduced with smaller current, increased number of LEDs in one channel, or fewer number of LED channels. It is noted that the conduction loss of the MOSFETs during the inductor charging period is excluded in the above study. Such energy loss is dependent on the duration of Mode 0.

The proposed structure can be used for tricolor system (RGB) and tetracolor system (RGBW or RGBA). However, some sophisticated gate drivers might be needed. During the time interval Δt_0 when the inductor is being charged, the LED channels are bypassed. Thus, the LED channels cannot be fully utilized, giving the limitation of the proposed method.

The buck-type SIMO LED driver with series-connected channel structure in [27] requires the input voltage being higher than the output voltage, giving the design challenge for the system with many series-connected LED channels. Moreover, a separate switching network is required to regulate the inductor current. Conversely, the proposed boost-type structure combines the channel bypass switches with the converter switch. Therefore, it does not require a high input voltage and also reduces the number of switches. A comparison among various structures with single inductor is shown in Table VI.

VI. CONCLUSION

An investigation into the use of single inductor for driving *N* series-connected LED channels is presented. Compared with the conventional architecture having all LED channels connected in parallel and $(N+1)$ switches, the proposed structure has the merits of 1) requiring *N* switches, 2) allowing all channels to be driven concurrently in every switching cycle, and 3) being insensitive to the duration of the transition switching from one channel to another. The concept has been demonstrated on a two-channel structure with tunable luminous flux and CCT. The experimental results are in close agreement with the theoretical predictions.

APPENDIX

A. Derivations of (17) and (32)

For the light emitted by an LED or LED module, (x_0, y_0) denotes the CIE 1931 chromaticity coordinates, X_0, Y_0, and Z_0 denote the tristimulus values, $\phi_{s,0}$ denotes its luminous flux, and β is a scale constant (683 lm/W). Based on [35]

$$X_0 = \frac{x_0}{y_0}\frac{\phi_{s,0}}{\beta} \tag{A.1}$$

$$Y_0 = \frac{\phi_{s,0}}{\beta} \tag{A.2}$$

$$Z_0 = \frac{1 - x_0 - y_0}{y_0}\frac{\phi_{s,0}}{\beta}. \tag{A.3}$$

For the light synthesized by *N* LED channels, its tristimulus values *X*, *Y*, and *Z* are

$$X = \sum_{i=1}^{N} X_i = \sum_{i=1}^{N} \frac{x_i}{y_i}\frac{\phi_{s,i}}{\beta} \tag{A.4}$$

$$Y = \sum_{i=1}^{N} Y_i = \sum_{i=1}^{N} \frac{\phi_{s,i}}{\beta} \tag{A.5}$$

$$Z = \sum_{i=1}^{N} Z_i = \sum_{i=1}^{N} \frac{1-x_i-y_i}{y_i}\frac{\phi_{s,i}}{\beta}. \tag{A.6}$$

By using (A.4)–(A.6)

$$X + Y + Z = \sum_{i=1}^{N} \frac{1}{y_i}\frac{\phi_{s,i}}{\beta}. \tag{A.7}$$

The color coordinates of the synthesized light (*x*, *y*) are

$$x = \frac{X}{X+Y+Z} = \frac{\sum_{i=1}^{N} \frac{x_i}{y_i}\phi_{s,i}}{\sum_{i=1}^{N} \frac{1}{y_i}\phi_{s,i}} \tag{A.8}$$

$$y = \frac{Y}{X+Y+Z} = \frac{\sum_{i=1}^{N} \phi_{s,i}}{\sum_{i=1}^{N} \frac{1}{y_i}\phi_{s,i}}. \tag{A.9}$$

The CCT of the synthesized light [36] is

$$\mathrm{CCT} = -437 \times A^3 + 3601 \times A^2 - 6831 \times A + 5514.31 \tag{A.10}$$

where

$$A = \frac{x - 0.329}{y - 0.187}. \tag{A.11}$$

Therefore, CCT_o is the function of luminous flux of each channel, that is

$$\mathrm{CCT}_o = \Im\left(\phi_{s,1},\ \phi_{s,2},\ \ldots,\ \phi_{s,N}\right). \tag{17}$$

For the case that the light is synthesized by two channels

$$\begin{aligned} A &= \frac{x - 0.329}{y - 0.187} \\ &= \frac{\frac{\frac{x_1}{y_1}\phi_{s,1} + \frac{x_2}{y_2}\phi_{s,2}}{\frac{1}{y_1}\phi_{s,1} + \frac{1}{y_2}\phi_{s,2}} - 0.329}{\frac{\phi_{s,1} + \phi_{s,2}}{\frac{1}{y_1}\phi_{s,1} + \frac{1}{y_2}\phi_{s,2}} - 0.187} \\ &= \frac{\frac{x_1 - 0.329}{y_1} + \frac{x_2 - 0.329}{y_2}\frac{\phi_{s,2}}{\phi_{s,1}}}{\frac{y_1 - 0.187}{y_1} + \frac{y_2 - 0.187}{y_2}\frac{\phi_{s,2}}{\phi_{s,1}}}. \end{aligned} \tag{A.11}$$

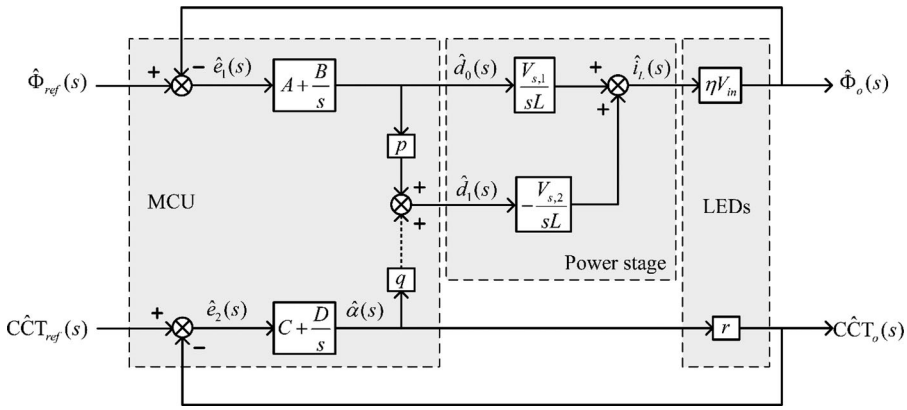

Fig. 16. Small-signal model of the two-loop control.

Therefore, CCT_o of the synthesized light is the function of the flux ratio

$$\mathrm{CCT}_o = \rho\left(\frac{\phi_{s,2}}{\phi_{s,1}}\right). \tag{32}$$

B. Proof of System Stability

According to Section II, there are three operating modes in each switching cycle. In Mode 0, $\Delta t_0 = d_0 T_s$, both MOSFETs are turned ON and the inductor is charged

$$L\frac{di_L}{dt} = V_{\text{in}}. \tag{A.13}$$

In Mode 1, $\Delta t_1 = d_1 T_s$, both MOSFETs are tuned OFF and the two LED channels are activated

$$L\frac{di_L}{dt} = V_{\text{in}} - V_{s,1} - V_{s,2}. \tag{A.14}$$

In Mode 2, $\Delta t_2 = d_2 T_s = (1 - d_0 - d_1)T_s$, the MOSFET across the LED channel 2 is turned ON

$$L\frac{di_L}{dt} = V_{\text{in}} - V_{s,1}. \tag{A.15}$$

Based on (A.13)–(A.15), a time-averaged equation can be shown to be

$$L\frac{d[i_L(t)]_{T_s}}{dt} = V_{in} - [1 - d_0(t)]V_{s,1} - d_1(t)V_{s,2} \tag{A.16}$$

By introducing small-signal variations into $i_L(t), d_0(t)$ and $d_1(t)$ and linearizing the equation

$$L\frac{d\hat{i}_L(t)}{dt} = \hat{d}_0(t)V_{s,1} - \hat{d}_1(t)V_{s,2} \tag{A.17}$$

where $\hat{i}_L(t), \hat{d}_0(t)$, and $\hat{d}_1(t)$ are the small-signal perturbations of $i_L(t), d_0(t)$, and $d_1(t)$.

Therefore, the small-signal models of the power conversion stage is

$$\frac{\hat{i}_L(s)}{\hat{d}_0(s)} = \frac{V_{s,1}}{sL} \tag{A.18}$$

and

$$\frac{\hat{i}_L(s)}{\hat{d}_1(s)} = -\frac{V_{s,2}}{sL}. \tag{A.19}$$

The small signal model of the two-loop control is shown in Fig. 16. $A + \frac{B}{s}$ and $C + \frac{D}{s}$ are the transfer functions of the PI controllers for the luminous flux control loop and CCT control loop, respectively. The relationships among $\hat{\alpha}(s), \hat{d}_0(s)$ and $\hat{d}_1(s)$ are related to (33) and (51).

For Scenario 1, $0 \le \alpha < 1, m = \alpha, d_1 = \alpha(1 - d_0)$

$$\hat{d}_1(s) = -\alpha_0 \hat{d}_0(s) + (1 - D_0)\hat{\alpha}(s) \tag{A.20}$$

in which α_0, D_0 are the steady-state values of α and d_0, respectively. Therefore, $p = -\alpha_0 (-1 < p \le 0)$ and $q = 1 - D_0$.

For Scenario 2, it is the same as Scenario 1, except that $\alpha = 1,\ p = -1$ and $q = 1 - D_0$.

For Scenario 3, $1 < \alpha \le 2,\ m = 2 - \alpha, d_1 = (2 - \alpha)(1 - d_0)$

$$\hat{d}_1(s) = (\alpha_0 - 2)\hat{d}_0(s) - (1 - D_0)\hat{\alpha}(s) \tag{A.21}$$

in which α_0 and D_0 are the steady-state value of α and d_0, respectively. Thus, $p = \alpha_0 - 2 (-1 < p \le 0)$ and $q = -(1 - D_0)$.

As $\Phi_o \approx \eta\, V_{\text{in}}\, \bar{I}_L$, the relationship between $\hat{\Phi}_o(s)$ and $\hat{i}_L(s)$

$$\hat{\Phi}_o(s) = \eta\, V_{\text{in}}\, \hat{i}_L(s). \tag{A.22}$$

According to (34) and (51), the relationships between $\hat{\mathrm{CCT}}_o(s)$ and $\hat{\alpha}(s)$ is linear, and the slope is represented by *r*.

Based on Fig. 16, the control of CCT is not affected by the luminous flux control loop, but the CCT control loop affects the luminous flux control. Since the CCT control loop is set much faster than the flux control, the CCT control will reach steady state much earlier than the flux control. Since the CCT control has reached its steady state, $\hat{\alpha}(s) = 0$, the CCT control loop will not affect the flux control. In this way, the control loops are decoupled. The stabilities of the decoupled control are studied. For the CCT control shown in Fig. 17(a), the closed-loop transfer

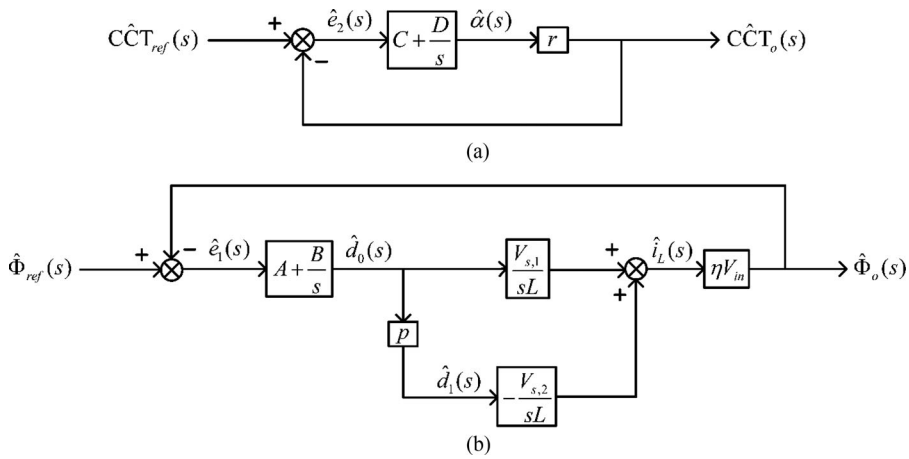

Fig. 17. Decoupled small-signal model. (a) CCT control. (b) Luminous flux control.

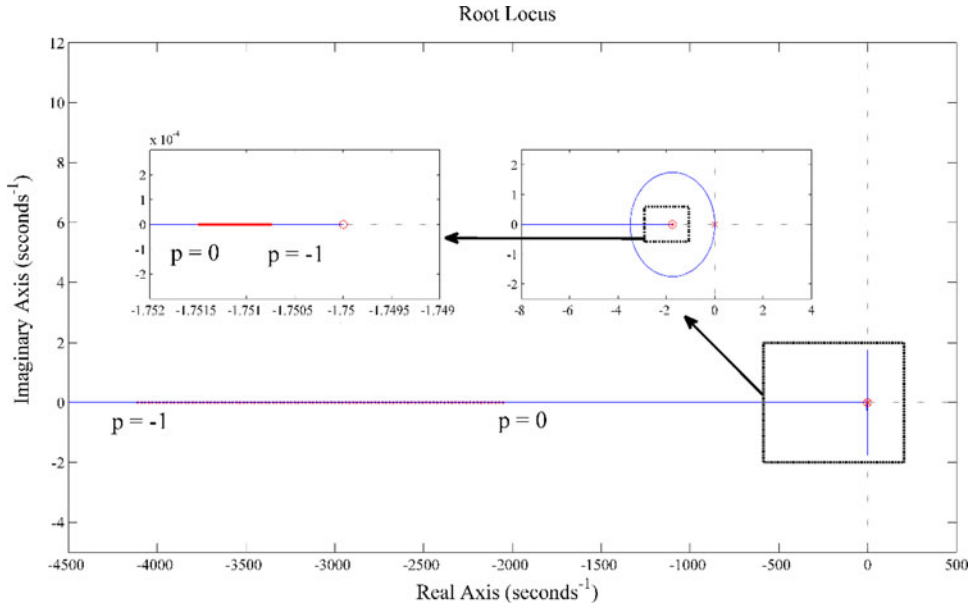

Fig. 18. Root locus of the flux control.

function is

$$\frac{\hat{C\hat{C}T}_o(s)}{\hat{C\hat{C}T}_{\rm ref}(s)} = \frac{r\,(C\,s\,+\,D)}{(1\,+\,r\,C)\,s\,+\,r\,D}. \tag{A.23}$$

The pole is $s = -\frac{r\,D}{1\,+\,r\,C}$. Since the values of r, C, and D are positive, the pole is on the left-half-plane. Thus, the CCT control loop is stable.

The decoupled flux control is shown in Fig. 17(b). The forward voltage of the cool and warm LEDs in the prototype is the same, that is $V_{s,1} = V_{s,2} = V_s$. The open-loop transfer function is $\frac{\eta\,V_{\rm in}\,V_s(1-p)(A\,s\,+\,B)}{L\,s^2}$. The closed-loop transfer function is

$$\frac{\hat{\Phi}_o(s)}{\hat{\Phi}_{\rm ref}(s)} = \frac{\eta\,V_{\rm in}\,V_s(1\,-\,p)(A\,s\,+\,B)}{L\,s^2\,+\,\eta\,V_{\rm in}\,V_s\,(1\,-\,p)(A\,s\,+\,B)}. \tag{A.24}$$

Fig. 18 shows the root locus of the flux control loop with change of $K(K = 1 - p)$. The big picture shows the whole root locus, and details of the part in the dot rectangular are shown in the arrow-guided picture. In this enlarged picture, details of the part in the dot rectangular are shown in the arrow-guided picture on the left. The starting points, $p = 0$, end points, $p = -1$, are labeled in the picture. Thus, the flux control loop is stable.

REFERENCES

[1] R. Zhang and H. Chung, "An overview of current-balancing techniques for paralleled LED strings," *IEEE Ind. Electron. Mag.*, vol. 9, no. 2, pp. 17–23, Jun. 2015.
[2] C. Branas, F. J. Azcondo, and J. M. Alonso, "Solid-state lighting: A system review," *IEEE Ind. Electron. Mag.*, vol. 7, no. 4, pp. 6–14, Dec. 2013.
[3] C. Wey, Y. C. Yeh, C. H. Sun, and T. S. Lee, "Driver and method for driving a semiconductor light emitting device array," U.S. Patent 7,605,809, Oct. 2009.
[4] U. Hu and M. Jovanovic, "LED driver with self-adaptive drive voltage," *IEEE Trans. Power Electron.*, vol. 23, no. 6, pp. 3116–3125, Nov. 2008.
[5] C. Yang, G. Lei, and Y. Lai, "Light emitting diode circuit having even current," U.S. Patent 7,675,240, Mar. 2010.

[6] S. Li, W. X. Zhong, W. Chen, and S. Y. R. Hui, "Novel self-configurable current-mirror techniques for reducing current imbalance in parallel light-emitting diode (LED) strings," *IEEE Trans. Power Electron.*, vol. 27, no. 4, pp. 2153–2162, Apr. 2012.
[7] G. P. Bouchard, "Floating switch controlling LED array segment," U.S. Patent 7,994,725, Aug. 2011.
[8] C. H. Lin, T. Y. Hung, C. M. Wang, and K. J. Pai, "A balancing strategy and implementation of current equalizer for high power LED backlighting," in *Proc. Int. Conf. Power Electron. Drive Syst.*, 2007, pp. 1613–1617.
[9] X. Qu, S. C. Wong, and C. K. Tse, "A current balancing scheme with high luminous efficacy for high-power LED lighting," *IEEE Trans. Power Electron.*, vol. 29, no. 6, pp. 2649–2654, Jun. 2014.
[10] H. Kim, C. Yoon, H. Ju, D. Jeong, and J. Kim, "An AC-powered, flicker-free, multi-channel LED driver with current-balancing SIMO buck topology for large area lighting applications," in *Proc. 29th Appl. Power Electron. Conf. Expo.*, Fort Worth, TX, USA, 2014, pp. 3337–3341.
[11] A. Lee, J. Sin, and P. Chan, "Scalability of quasi-hysteretic FSM-based digitally controlled single-inductor dual-string buck LED driver to multiple strings," *IEEE Trans. Power Electron.*, vol. 29, no. 1, pp. 501–513, Jan. 2014.
[12] H. Chen, Y. Zhang, and D. Ma, "A SIMO parallel-string driver IC for dimmable LED backlighting with local bus voltage optimization and single time-shared regulation loop," *IEEE Trans. Power Electron.*, vol. 27, no. 1, pp. 452–462, Jan. 2012.
[13] S. Dietrich, S. Strache, R. Wunderlich, and S. Heinen, "Get the LED out: Experimental validation of a capacitor-free single-inductor, multiple-output LED driver topology," *IEEE Ind. Electron. Mag.*, vol. 9, no. 2, pp. 24–35, Jun. 2015.
[14] K. Modepalli and L. Parsa, "A scalable N-color LED driver using single inductor multiple current output topology," *IEEE Trans. Power Electron.*, vol. 31, no. 5, pp. 3773–3783, May 2016.
[15] M. M. Sisto and J. Gauvin, "Accurate chromatic control and color rendering optimization in LED lighting systems using junction temperature feedback," *Proc. SPIE*, vol. 9190, Sep. 2014, Art. no. 919002.
[16] X. Qu, S. Wong, and C. Tse, "Color control system for RGB LED light sources using junction temperature measurement," in *Proc. IEEE Ind. Electron. Soc.*, Nov. 2007, pp. 1363–1368.
[17] A. Lee, H. Chen, S. Tan, and S. Hui, "Precise dimming and color control of LED systems based on color mixing," *IEEE Trans. Power Electron.*, vol. 31, no. 1, pp. 65–80, Jan. 2016.
[18] S. K. Ng, K. H. Loo, Y. M. Lai, and C. K. Tse, "Color control system for RGB LED with application to light sources suffering from prolonged aging," *IEEE Trans. Ind. Electron.*, vol. 61, no. 4, pp. 1788–1798, Apr. 2014.
[19] S. Muthu and J. Gaines, "Red, green, and blue LED based white light source: Implementation challenges and control design," in *Proc. Ind. Appl. Conf.*, Oct. 2003, pp. 515–522.
[20] A. Gulati, "The science behind color mixing," Feb. 2014. [Online]. Available: www.cypress.com/file/114061/download
[21] F. Wang, C. Tang, and B. Huang, "Multivariable robust control for a red-green-blue LED lighting system," *IEEE Trans. Power Electron.*, vol. 25, no. 2, pp. 417–428, Feb. 2010.
[22] D. Ma, W. Ki, C. Tsui, and P. Mok, "Single-inductor multiple-output switching converters with time-multiplexing control in discontinuous conduction mode," *IEEE J. Solid-State Circuits*, vol. 38, no. 1, pp. 89–100, Jan. 2003.
[23] D. Ma, W. Ki, and C. Tsui, "A pseudo-CCM/DCM SIMO switching converter with freewheel switching," *IEEE J. Solid-State Circuits*, vol. 38, no. 6, pp. 1007–1014, Jun. 2003.
[24] K. Seol, Y. Woo, G. Cho, G. Gho, and J. Lee, "A synchronous multioutput step-up/down dc–dc converter with return current control," *IEEE Trans. Circuits Syst. II, Exp. Briefs*, vol. 56, no. 3, pp. 210–214, Mar. 2009.
[25] Y. Moon, Moon, Y. Roh, J. Gong, and C. Yoo, "Load-independent current control technique of a single-inductor multiple-output switching DC–DC converter," *IEEE Trans. Circuits Syst. II*, vol. 59, no. 1, pp. 50–54, Jan. 2012.
[26] Y. Hsieh and Y. Juang, "Analysis and suppression of overcurrent in boost LED drivers," *J. Display Technol.*, vol. 9, no. 5, pp. 388–395, May 2013.
[27] H. Yang *et al.*, "A 96%-efficiency and 0.5%-current-cross- regulation single-inductor multiple floating- output led driver with 24b color resolution," in *Proc. Int. Solid-State Circuits Conf.*, 2016, pp. 230–231.
[28] X. Li, "Fundamental of photometry and colorimetry," (in Chinese) in *Engineering Optics*, 1st ed., Beijing, China: Science Press, 2005, pp. 134–135.
[29] S. Singh, "Impact of color on marketing," *Manag. Decision*, vol. 44, pp. 783–789. 2006.
[30] A. Sedra and K. Smith, *Microelectronic Circuits*. London, U.K.: Oxford Univ. Press, 2004.
[31] "TCS3472 Color Light-to-Digital Converter with IR Filter," Texas Adv. Optoelectron. Solut., Plano, TX, USA, 2012.
[32] H. Burton, "DN40-Lux and CCT Calculations using ams Color Sensors," ams AG, Aug. 2013.
[33] A. Baker, "ANSI C78.377-201x revision: New nominal CCTs, smaller quadrangles and circles," May 2014. [Online]. Available: https://www.americanlightingassoc.com/Downloads/Engineering/Engineering-2014/13–1a-Baker-RevLEDChromaticityStd.aspx
[34] B. Hauke, "Basic calculation of a boost converter's power stage," Jan. 2014. [Online]. Available: http://www.ti.com/lit/an/slva372c/slva372c.pdf
[35] H. Zhao and S. Lee, "Determination of driving current of RGB LEDs for white light illumination," in *Proc. 13th Int. Conf. Electron. Packag. Technol. High Density Packag.*, 2012, pp. 1540–1545.
[36] C. Dai and J. Yu, "Discussion on the calculating methods for color temperature of the source," *ACTA Metrologica Sinca*, vol. 21, no. 3, pp. 183–188, 2000.

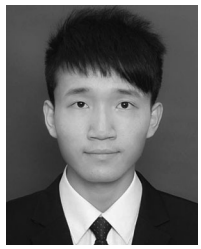

Xiaoqing Zhan (S'16) received the B.Eng. degree in electrical engineering from the Huazhong University of Science and Technology, Wuhan, China, in 2014. He is currently working toward the Ph.D. degree in Department of Electronic Engineering, City University of Hong Kong, Kowloon, Hong Kong.

His research interests include LED lighting system and power converters.

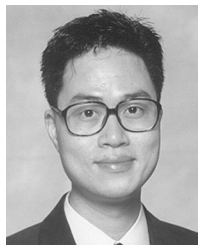

Henry Shu-Hung Chung (M'95–SM'03–F'16) received the B.Eng. and Ph.D. degrees in electrical engineering from the Hong Kong Polytechnic University, Kowloon, Hong Kong, in 1991 and 1994, respectively.

Since 1995, he has been with the City University of Hong Kong, Kowloon, where he is currently a Professor in the Department of Electronic Engineering and the Director of the Center for Smart Energy Conversion and Utilization Research. His current research interests include renewable energy conversion technologies, lighting technologies, smart grid technologies, and computational intelligence for power electronic systems. He has edited 1 book, authored 8 research book chapters, and over 350 technical papers including 170 refereed journal papers in his research areas, and holds 35 patents.

Dr. Chung was the Chair of the Technical Committee of the High-Performance and Emerging Technologies, IEEE Power Electronics Society in 2010–2014. He is currently an Editor-in-Chief of the IEEE Power Electronics Letters and the Associate Editor of the IEEE TRANSACTIONS ON POWER ELECTRONICS and the IEEE JOURNAL OF EMERGING AND SELECTED TOPICS IN POWER ELECTRONICS. He has received numerous industrial awards for his invented energy saving technologies.

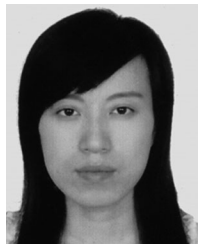

Ruihong Zhang (S'12–M'14) received the B.Eng. degree in computer science and the M.Eng. degree in electrical engineering, in 2005 and 2008, respectively, from Harbin Institute of Technology, Harbin, China, and the Ph.D degree from City University of Hong Kong, Kowloon Tong, Hong Kong, in 2013.

She is currently an Associate Professor at Northwestern Polytechnical University, Xi'an, China. Her current research interests include the lighting system, power-factor-correction, resonant converters, ac/dc, dc/dc converters, and energy-recycling techniques.